


NATIONAL AERONAUTICS AND SPACE ADMINISTRATION
NASA Contract NASr-217

A STUDY OF INJECTOR SPRAY CHARACTERISTICS
IN A SIMULATED ROCKET COMBUSTION CHAMBER
INCLUDING LONGITUDINAL MODE PRESSURE
OSCILLATIONS

Technical Report No. 730
Department of Aerospace and Mechanical Sciences


Prepared by:


Dennis A. Gary
Assistant-in-Research

Approved by:


Luigi Crocco
Robert H. Goddard Professor
of Aerospace Propulsion

and


David T. Harrje
Senior Research Engineer

Reproduction, translation, publication, use and disposal in whole or
part by or for the United States Government is permitted.

June 1966

Guggenheim Laboratories for the Aerospace Propulsion Sciences
PRINCETON UNIVERSITY
Princeton, New Jersey

I. SUMMARY

Thirty-five (35) sets of number size droplet counts were taken. These data were obtained from various 90° impinging jet injectors in ambient pressures up to 100 psig and pressure drops across the injectors of up to 100 psia. Further, they were conducted in both constant ambient pressure and oscillating pressure with peak-to-peak values which were 5% of the mean ambient pressure. The distributions were compared by representative curves which had been fitted to the data.

In any such comparison of number size data the variations in the total count of drops necessitates a conversion of the count data from absolute values to a percentage of the total count. Thus, just as the sum of these percentage counts must be unity, the integral (over all possible values of diameter) of any representative curve must also be unity. If this "normalizing condition" is not satisfied, the constants of the equation are more like those of any algebraic equation which can be fitted to the data rather than representing the data and bearing a physical significance.

Satisfying this condition is the task of the constant, α , in the most general form of the distribution equations:

$$\frac{dN}{dD} = \alpha f(D) \quad (1.1)$$

Knowing the limits of N (0 to 1 since it is a percentage) and of D (0 to ∞ or some upper limit) the value of α can be obtained by numerical integration. In only one of the three representative curves considered (the so-called Nukiyama Tanasawa) is this integration analytic.

Because of its analytic evaluation of α and the fact that it has only one curve fitting constant, the Nukiyama Tanasawa Equation could be fitted to the data by an iterative method. However, the other two representative curves (log probability and upper limit probability) were found to be fitted to the data more easily by simple trial and error. Thus, computer programs were written to achieve these fits by the respective methods.

Although all three distribution equations were found to successfully fit the data, the upper limit probability equation was found to be most satisfactory for two reasons. First, its constants and parameters are easily interpreted in terms of their effect on the curve shape. Secondly, it was possible to predict the actual D_{30} of the spray more accurately than the other curves because it is a more realistic fit with counts only up to a certain maximum size.

The data from the test runs was fitted by the upper limit probability curve and then analyzed. The results found no changes in distributions which were dependent upon the operating conditions. The only differences which were found were attributable to a population density wave phenomenon which was found. While similar in nature to that observed by other investigators it was of a much lower frequency (100 cps compared to 2000 or 3000 cps). This low frequency resulted in such a long wave length (3 1/2") that the photographs from which the distributions were taken corresponded to dense and rarified sections of the wave. It was these photographs which showed the differences in the shape of the drop size distributions.

II TABLE OF CONTENTS

I	SUMMARY	1
II	TABLE OF CONTENTS	3
III	ACKNOWLEDGMENTS	4
IV	SYMBOL TABLE	5
V	INTRODUCTION	8
VI	EXPERIMENTAL APPARATUS	10
	Testing Facilities	10
	Recording Apparatus	12
VII	DATA REDUCTION	17
	Imposed Multimodal Counting Error	17
	Sizes of Templates	17
	Irregularly Shaped Droplets	17
	Camera Depth of Field and Droplet Size	18
	Depth of Field Correction	21
VIII	DATA PROCESSING	22
	Normalization	22
	Standard Diameter Increments	23
	Regrouping of Data Points	25
	Number-Volume Relations	27
	Characteristic Diameters	29
	General Comments of Distribution Curves	31
	Evaluating Successfulness of Curve Representations	32
	The Distribution Curves	34
	Probability Equations	34
	Nukiyama-Tanasawa Equations	36
	Linear Curve Fits	39
	Attempt to Use Least Square Curve Fit	41
	Nonlinear Least Square Curve Fit	43
	Multimodal Distributions	46
IX	RESULTS AND CONCLUSIONS	47
	Best Fitting Curve	47
	Interpreting the Upper Limit Curves	48
	Droplet Wave Phenomenon	49
	Longitudinal Resonant Pressure Oscillations	52
	Longitudinal Locations	52
	Injector Pressure Drop	52
	Chamber Pressure	53
	Prediction of D_{30}	54
	Concluding Remarks	54
X	REFERENCES	56
	FIGURES	
	DISTRIBUTION LIST	

III. FORWARD AND ACKNOWLEDGEMENTS

This technical report represents a continuation of the study on the spray characteristics of impinging liquid jets originally outlined in the Princeton University Department of Aerospace and Mechanical Sciences Technical Report No. 648 "Evaluation of a Light Scattering Technique for Determining the Spray Characteristics of Impinging Liquid Jets" (Author Hans Bredfeldt, March 1964). Direct photographic techniques have been employed in the current study based on the shortcomings of the light scattering technique previously used. The droplet population variations, which are reported here, are being studied further and a preliminary status report is available in this year's annual report (Report 553-f).

Support for this research was provided under NASA Grant NsG 99-60 and NASA Contract NASr-217. In addition, data reduction involved the use of the computer facilities supported in part by the National Science Foundation under Grant NSF-GP 579.

Working closely with Mr. Gary on the data reduction and experimental apparatus was Mr. Victor Warshaw together with other members of the Guggenheim Laboratories Staff. The majority of tests on and the results from a streak camera were due to the efforts of Mr. Terry Brubaker, a Princeton undergraduate at the time. Mr. Dan Leh and Mr. Lanny Hoffman of the Guggenheim Computer Group provided able assistance in the computations involving IBM 1620 and 7094 equipment.

D.T.H.

IV. SYMBOL TABLE

a	= The normalizing constant of the conventional probability equation.
A	= The normalizing constant of the Nukiyama-Tanasawa Equation.
α	= A general representation for all normalizing constants.
b	= The normalizing constant of the log probability equation; a dependent constant.
B	= The Y intercept of a linearized curve distribution.
c	= The normalizing constant of the upper limit probability equation.
C	= An exponential constant; the only independent constant in the Nukiyama-Tanasawa Equation.
γ	= A standard deviation constant; one of two independent constants in the upper limit probability equation.
d	= The differential operator.
D	= The diameter of droplets.
D_f	= The droplet diameter for which a camera's depth of field equals the spray width.
D_i	= Injector jet diameter.
$D_{vw}, D_{10}, \text{etc.}$	= Characteristic diameters (defined Section VIII, "Characteristic Diameters")
D_M	= The maximum diameter or upper limit diameter; one of two independent constants in the upper limit probability equation.
D_{mode}	= The diameter at the modal point of a curve distribution.
δ	= A standard (or average) deviation; one of two independent constants in the conventional probability equation.
Δ	= The incremental operator.
e	= The natural logarithm base = 2.71828.
E	= The total square error between a point and curve distribution.
ξ	= A graphical area error between a point and curve distribution.

$f = f(D)$	= A general representation for all distribution functions, excluding the normalizing constant, α .
F	= The aperture diameter in a camera lens.
G	= The slope of a linearized curve distribution.
k	= The constant which is assumed to linearly relate the circle of confusion to droplet diameters.
ℓ	= Total number of points in a real point distribution.
m	= Total number of droplets in an imaginary characteristic spray.
M	= An average diameter constant; one of two independent constants in the log probability equation.
n_k	= The actual count of droplets of diameter D_k ; integer values only.
N_k	= The percent of the total number of droplets which have diameters <u>less</u> than or equal to D_k .
o	= The circle of confusion.
p	= One of two parameters of the Nukiyama-Tanasawa Equation.
P	= The chamber pressure, psi.
π	= 3.14159
q	= One of two parameters of the Nukiyama-Tanasawa Equation.
R_k	= The percentage of the total volume of droplets which have diameters less than D_k .
ρ	= Liquid density.
s	= The only parameter in the upper limit probability equation.
S	= The object distance from a camera.
ΔS	= The depth of field of a camera on an object.
σ	= A standard deviation constant; one of two independent constants of the log probability equation.
v_i	= Velocity of injector jet.
W_i	= $\frac{\Delta N_i}{\Delta D_i}$ a defined simplifying substitution.
x	= Longitudinal distance downstream of injector.

- X = The transformed D variable in a linearized distribution.
- y = $C D^q$ = an integration substitution.
- Y = The transformed $\frac{dN}{dD}$ or $\frac{\Delta N}{\Delta D}$ variable in a linearized distribution.
- Z = The magnification of a camera system.

CONVENTIONS

$$\Gamma_n = \int_0^{\infty} e^{-x} x^{n-1} dx = \text{The complete gamma function of } n.$$

$$\sum (\text{no limits}) = \sum_{i=1}^{\ell}$$

$$\int dN (\text{no limits}) = \int_0^1 dN$$

$$\int dD (\text{no limits}) = \int_0^{\infty} dD$$

V. INTRODUCTION

The investigation of characteristics of liquid sprays has a long history in engineering and particularly in the study of combustion. Much of the earliest work was directed toward the fuel injection and combustion of internal combustion engines.¹ More recently these efforts have been directed to the combustion processes in liquid rocket engines.

Here at Princeton there is a research effort in liquid rocket combustion instability in which studies of this nature are of importance.² In particular it is desirable to determine whether a mechanism exists which couples spray characteristics with acoustic chamber pressure oscillations. If such a mechanism can be shown to exist then perhaps a theoretical injection model can be constructed which will aid in the prediction and thus avoidance of unstable injection configurations.

Though obviously the ideal testing procedure would be to conduct the tests on an actual rocket engine, the high temperature, high pressure and combustion luminescence create rather severe experimental problems. In spite of this, some work has been done under actual rocket conditions.³ The expense and problems associated with such tests, however, make it desirable to be able to obtain similar data from a simulated cold flow chamber.

The sophistication of such cold flow devices can vary from a simple atmospheric spray to a geometrically similar, pressurized "combustion chamber" with an imposed flow of gas. The pressurization of such a chamber is intended to duplicate the densities of the combustion gases of an actual rocket chamber while the flow of gas is intended to simulate the generation of these combustion products. The simulation of combustion instability can be achieved by exhausting the gas through a siren such that resonant acoustic waves are set up in the chamber.

The experimental part of this work was done on a chamber which does include pressurization, imposed gas flow and optional siren exhaust in its simulation.

The two spray properties which were studied in this work are the number size distribution and characteristic diameters. The distributions are significant in combustion processes since the energy released and its rate of release from any one fuel are both functions of the size of the droplet. Thus, the combined effect on combustion of a group of droplets (i.e. the combustion characteristics of a spray) will vary from one distribution to another depending on the number and sizes of droplets in the spray.⁴ For the same mass of propellant the increased surface area provided by a droplet distribution containing a proportionately greater amount of the smaller droplets naturally results in a more rapid burning rate. The location of this combustion as well as the gradient influences both steady and unsteady combustion.

Along with number-size distribution studies in the past an associated curve fitting technology has developed. Several different equations have been suggested and used to represent the data.^{1,5,6} These curves serve as an analytical representation of the spray characteristics, and when properly determined can relieve the problems associated with data scatter and thus provide, from the associated constants, an improved physical model of distribution variations. A complete review of these equations and the methods of fitting them to the data is covered in this work. Furthermore, an evaluation of the success of the representation of a real point distribution by each of the representative curve distributions is presented.

For the reader's benefit this work is divided into 10 roman numbered "sections" some of which are subdivided into titled "topics". All of these are listed in the table of contents (Section II). References to preceding or following topics refer to those within the section unless otherwise stated. The equations are numbered for quick reference with the integer referring to the page number and the decimal referring to the specific equation on that page.

VI. EXPERIMENTAL APPARATUS

As in most experimental investigations the apparatus used in this work can conveniently be divided into two parts: 1) the testing facilities and 2) the recording apparatus. In this case the testing facilities include a cold flow chamber which is designed to simulate conditions within a combustion chamber, the associated gas and liquid flow systems which feed the chamber and the siren exhausting system used to produce the pressure oscillations in the chamber. The recording apparatus includes the various cameras which take the actual data, the associated lighting systems, the flow metering devices for both the gas and liquid injected into the chamber and finally, the system for recording the chamber conditions when the photographs are taken. A photograph of the testing chamber, the camera and the lighting system is shown in Figure 1.

Testing Facilities

A schematic of the simulated combustion chamber appears in Figure 2 and a photograph of the chamber from the same angle follows in Figure 3. It is a 6.127" (i.d.) horizontal cylindrical chamber with a 6½" long test section. Mounted on each side of this test section are three pairs of quartz windows aligned to give a 1" circular view perpendicular to and through the chamber axis at the points 1/2", 2 1/8", and 3 3/4" downstream of the injection end. Next to the test section is a plexiglass section of identical internal geometry. By selecting various lengths for the plexiglass section the overall length and hence longitudinal resonant frequency of the chamber can be varied. However, only a 13" chamber length with an associated frequency of 530 cps was used in these tests.

The injector (or pair of injectors) was mounted in the center of one end of the test section. All of the injector elements tested were of a similar design (Figure 4) and have been used in other phases of the instability research which include rocket test firings. They are 90° like-on-like impinging jet injectors ("doublets") with orifice diameters

of .040, .059, .120, and .170 inches. In addition to these single doublets, a pair of .059 doublets 1/4" apart were also tested. Since impinging jet spray fans are not symmetrical, a choice had to be made on the relative fan positions. The elliptical fans were placed so that their major axes were colinear, referred to as zero spacing in Reference 2.

Originally the inlets for the nitrogen gas used in simulating the combustion products were spaced around the injector. However, early attempts at gathering data soon revealed that the windows were not sufficiently protected from the spray to keep them dry enough for photographic purposes. As a result, the injection of nitrogen was redesigned to use a circumferential slot which directed flow radially across the window surfaces before the nitrogen entered the resonating chamber. This method proved quite successful with only limited problems remaining on isolated tests on the furthest window downstream. The use of side injection of nitrogen into the resonating chamber also may have helped to simulate the generation of combustion products from adjacent injector elements.

The nitrogen came from a 1600 psi supply line and cooled significantly when expanded into the chamber. Thus, before being injected the nitrogen had to be heated through a hot water heat exchanger. This not only kept the expanding gas from dropping the chamber temperature below 32°F possibly forming ice in the photographic view, but also prevented external condensation from fogging the chamber windows. Operating chamber temperatures were in the neighborhood of ambient temperature.

The nitrogen was exhausted through a six hole siren in the exhaust end of the chamber. For steady-state runs the siren was clamped open, while during oscillating pressure runs it was driven by an electric motor through a varidrive which allowed the selection of the frequency of oscillation. The resonant frequency was determined by monitoring a pressure transducer output on an oscilloscope and adjusting the varidrive to maximize the pressure oscillation amplitude in the chamber. A seventh nitrogen outlet was added in order to keep the total gas flow constant during comparable runs under steady-state and oscillating pressure conditions. The size of this outlet was controlled by a hand valve.

This outlet did not feed through the siren and therefore had to be used exclusively in steady-state runs. This made a greater total exhaust area. However, since the gas flow rate through each of the other exhausting outlets is greater while the siren is clamped open (for steady-state) than when it is running, fewer outlets are needed for the same total flow rates during the steady-state runs than for the oscillating pressure. Therefore, several exhausting outlets had to be closed after the oscillating pressure runs and before the hand valve was used in the steady-state runs. This was accomplished by inserting aluminum plugs into the entrances to the outlets.

Thus, in any pair of test runs it was necessary to run the oscillating pressure test first. During these runs a number of exhaust holes were open, the siren was running and the gas flow was measured. Then, after some of the exhaust holes were plugged and the siren clamped open, the steady-state tests were run using the hand valve outlet to adjust the nitrogen flow rate to that measured during the oscillating pressure run. The gas flow rate was a function of the chamber pressure and the number of holes left open for the initial siren run. A minimum gas flow was necessary to keep the windows clean. The attainment of evenly distributed exit area was also considered. These factors resulted in the selection of four holes open for the siren runs. Subsequently, three holes open plus the valved outlet were needed for the steady-state runs.

All of the water entered the chamber from a nitrogen pressurized tank through the injector. It was then exhausted through a hole at the siren end and near the bottom of the chamber. The tank had a pressure limit of 500 psi and a capacity of 25 gallons. Both of these values proved adequate for the data taken. However, for the larger injectors the tank had to be refilled after each 2 or 3 minute test run.

Recording Apparatus

The camera was simply a 41" tube with a f-3.5, 200 mm lens mounted at one end and a Beattie 70 mm automatic film advance cartridge at the other. With the lens focus fixed at " ∞ " and the lens to film distance invariable, a constant magnification was obtained for all photographs

(5.2 times). Furthermore, with this arrangement the precise distance from the lens to the point of best focus was fixed and easily obtained. A slide of glass spheres (covering a range of sizes similar to actual droplet diameters later photographed) was prepared and mounted in the center of the chamber. By photographing these spheres through the test section windows (which alter the effective lens to object distance) the location of best focus for the spray centerline was found. Subsequent placement of the camera forward or backward would then give data for any desired spray location relative to the centerline.

Furthermore, by mounting a gauge micrometer on the camera and taking photographs of the glass spheres at incremental distances from the centerline best focus location, the depth of field calibration of the camera was obtained.

The choice of the final value of magnification of the camera system was based on a compromise of several variables. For a given film grain size, as the magnification increases smaller and smaller objects (in these case droplets) can be recorded. However, there are three limitations to the maximum magnification.

The first comes from a consideration of the inverse relationship between depth of field and magnification (Section VII, Equation (19.4)). For larger magnifications, if the depth of field becomes too small, the number of photographs which must be taken to obtain a large enough droplet count becomes excessively large. This leads to cumbersome and time consuming dark room and data reduction work. Although this did not become a serious problem, it does have further implications which are discussed in Section VII.

The second limitation arises from the need to maintain proper exposure. As the magnification increases so does the distance between the lens and film, and therefore, the exposure necessary for the same photographic quality. Since the time of exposure is determined by the speed necessary to stop the motion of the droplets, this limitation is really dependent upon the light source intensity. With sufficiently fast films the magnification used would have easily fit within the exposure limits. However, based on the film chosen for this work (see next page) the magnification used was nearly the maximum possible and couldn't have been significantly increased without additional problems.

The most important limitation concerned the overall size of the camera system. The test laboratory which houses the entire apparatus is of relatively limited space. Since the other two limitations were not critical the camera size (and hence magnification) was designed to make the most convenient use of the space available.

The final magnification selected was 5.2 times normal size. This proved to be adequate in resolving $10\ \mu$ diameter droplets which were sufficiently small to reveal the distribution characteristics of all injectors studied. However, similar studies on smaller injectors (e.g. .020") may necessitate even greater magnifications.

The choice of film and development was dependent upon photographically satisfying two conditions. The droplets have to be photographed 1) under lighting conditions which vary with different optical spray depths and 2) with sufficient contrast to quickly and accurately permit measurement of a droplet image from the resulting photograph. Since films with high contrast have, in general, small exposure latitudes, these two conditions cannot be satisfied by the choice of film alone. Therefore tests were conducted to determine the optimum film-developer combination. The final procedure used Kodak Plus-X Portrait Film (because of its fine grain and wide exposure latitude) developed in Kodak D-8 developer (providing high contrast). The negatives were then enlarged to a final magnification of about 30 on Kodak Polycontrast A paper. Although a number four filter would seem to be appropriate for this work to obtain added contrast, it was found that sufficient contrast had already been obtained by using the D-8 developer and that adding the filter to the printing process gave little if any improvement in contrast. Because of the longer exposures needed with the filter it was decided to save darkroom processing time by using no filter ("0" grade paper).

Since direct photography was used, as opposed to shadowgraph or Schlieren technique, the lighting system did not need to be collimated. However, as mentioned above, because of the long focal length of the camera, care had to be taken to obtain the maximum light for the exposure.

The light source that was finally decided upon used the spark from a 15 kv capacitor discharge of about 1 microsecond duration. The

light was concentrated into a diffused beam by placing the spark near the focal point of a single element acromatic lens. It was then passed through the spray and directly into the camera lens. This back lighting of the droplets, combined with the photographic processes previously discussed, provided excellent photographic contrast. The duration of the spark and therefore of the exposure is sufficiently short to stop all droplet motion in the data taken. It is expected, however, that at injector pressure drops higher than the standard condition (50 psi) slight blurring of the droplets due to their motion would be encountered. This would occur especially at locations closer to the injector face.

The capacitor recharging time of about 5 seconds proved to be the limiting factor in determining how rapidly the data could be taken.

A modified streak camera was adapted to the photographic set-up described previously by replacing the 70 mm Beattie film cartridge with a light tight box in which a 30" continuous loop of 35 mm film could be brought up to speeds of 1100 in/sec. The continuous loop concept is intended to conserve film (and subsequent development and processing time) by allowing the film to come to the proper speed before the exposure is made.

Since a continuous light source is needed for this camera a Mercury arc lamp was used. This lamp gave less intense light than the spark source so that a faster film had to be used. Since the data from this camera is concerned only with traces of the droplets and not with precise measurements of their sizes, contrast was no longer a serious problem. Kodak Royal-X Recording Film developed by standard procedures as recommended by the manufacturer was used.

This streak camera was used primarily to study waves of droplets (the so-called "Christmas Tree" effect). This was accomplished by running the film at a speed slow enough for the droplet images to trace paths of nearly 90° across the film rather than 45° as is usually desired in velocity studies. The result is a compact trace of droplets over relatively longer periods of time than in velocity studies.

The camera and lighting system were built in such a way that they could be moved to any one of the three windows by linear actuators

while the test was in progress. Furthermore, the camera was constructed to allow an additional linear actuator to move it perpendicular to the axis of the chamber in order to obtain data at various locations in the spray cross section.

The nitrogen flow rates were measured by the upstream conditions in an assumed isentropic choked nozzle. In the early runs the water flow rates were assumed constant through an injector for a constant pressure drop across it. Later a Pottermeter was installed for those injectors which had flow rates large enough to be accurately measured by it. Even more recently an electromagnetic flow meter was installed on the water inlet line.

The feed system pressures and chamber pressures were hand recorded from standard pressure gauges while the oscillating pressure in the "unstable" chamber runs was recorded via a Kistler 601 transducer displayed on an oscilloscope and photographed. The discharge of the spark light source gave an interference "blip" which revealed the time in the pressure oscillation cycle at which the spray photograph was taken.

VII. DATA REDUCTION

Once the tests were run, the photographic data had to be reduced to a more meaningful statistical form. As mentioned, one method chosen for studying these sprays is that of comparing number size distributions. Thus, the task of obtaining this statistical information is one of sizing and counting each individual droplet on any one photograph.

The method used to achieve this was direct comparison of each droplet image to five rows of ten circles of linearly increasing sizes in a clear plastic template. Once the best fitting circle was chosen an additional count for that size was recorded and the particular droplet marked so that it would not be recounted.

Imposed Multimodal Counting Error

However, subconscious preferences to avoid the template holes at the ends of each row were found to cause extraneous modal distributions in some of the data. Such counting preferences were proven to be the source of these modal results when recounts of the photographic data were made using a revised procedure. For the recount the edges of each droplet were first marked on the photograph and then the distance between the two marks was measured. The point distributions and fitted curves of both an original multimodal distribution and the corresponding recounted distribution from the same photograph are shown as distributions 252 and 257 respectively in Figure 8. A wedge comparator was used in conjunction with the droplet edge markings for the recount and for all counts thereafter.

Sizes of Templates

Both the circular and wedge comparators had 50 sizes in approximately constant increments up to .5" diameter. Since the photographs had magnifications of approximately 30 times actual size, these template holes corresponded to about 8μ increments up to a 400μ diameter.

Irregularly Shaped Droplets

In some of the tests ligaments of water of elliptical and odd

shaped droplets were photographed. An attempt was made to measure those parts of the ligaments which appeared to be forming into individual droplets and also to measure a large droplet as two or more if it appeared to be in the process of breaking up. Such measurements involve, of course, a subjective evaluation of the size of each forming "droplet". However, the important thing to note is that although the surface tension of the liquid may pull these potential droplets back into place, they do exhibit the same diameter and nearly the same surface area and volume as a completed droplet of the same size. Therefore, since they have nearly the same physical properties, it could be assumed that they would contribute to the combustion of the spray in the same way that a real droplet of that size would. If the surface tension does in fact pull them back into the main body of liquid instead of allowing them to form separate droplets, then this action and its effect on the combustion of the spray should show up in the studies of the number-size distributions taken further downstream.

This, in fact, is one of the main reasons why hand counts were used rather than machine counts in reducing the data. The droplets photographed had to be of nearly perfect circular shapes to be able to get reliable results from automatic droplet counters, except for the prohibitively expensive counters. This limitation would immediately eliminate studies on the larger size injectors and on smaller injectors at the first one or two windows since ligaments were still found under these conditions. Only droplets and ligaments appeared to form in the spray studies here. Apparently the impingement velocities were too great to allow sheets of liquid to form.⁷

Camera Depth of Field and Droplet Size

Although the previous topics cover the data reduction procedures actually used on the data presented in this report, there is one point which must be considered in any future use of these data. It is of particular interest should these data ever be compared to other number size spray distributions. The rest of this section is devoted to a discussion of this point.

It is well known that any camera has a depth of field which is dependent upon the desired circle of confusion. In measuring droplet

sizes, however, the tolerable circle of confusion is a function of the droplet size (smaller droplets need a smaller absolute error than larger droplets if the same relative error in droplet size is to be maintained). Thus, a number-size distribution obtained from a camera photograph is based on a count of droplets in a volume (the area seen by the camera times the depth of field) which is different for each size droplet.

The problem arises when we consider the possibility of variations across the spray in population densities of a particular size droplet. The point is not so much a desire to discern such variations, which certainly could prove interesting, but rather a desire to make a distribution represent the same volume for all size droplets. It is particularly desirable to avoid a situation where the smaller droplets represent a limited section of the spray while the larger droplets are sampled from the entire cross section. The smaller sections could have number-size distributions which are different from the total cross section distribution.

A theoretical relationship between the depth of field and droplet size can be obtained starting with a relationship between depth of field and circle of confusion (Reference 8):

$$\Delta S = \frac{2S}{\frac{ZF}{o} - \frac{o}{ZF}} \quad (19.1)$$

where the depth of field is ΔS , object distance is S , magnification is Z , aperture is F , and tolerable circle of confusion is o . For the values of o encountered in these tests, however, the second term in the denominator may be neglected giving a linear relationship:

$$\Delta S = \frac{2S}{ZF} o \quad (19.2)$$

Thus, if it is assumed that the circle of confusion is a linear function of the size of the droplet or glass bead (which is equivalent to saying that the same relative error is allowed in measuring each droplet):

$$o = kD \quad (19.3)$$

$$\Delta S = \frac{2S}{ZF} kD \quad (19.4)$$

The depth of field testing procedure discussed earlier (Section VI, "Experimental Apparatus") was used to verify this linear result and solve for the value of k . The result of these tests is:

$$\Delta S = .0024 D \quad (20.1)$$

where ΔS is in inches and D in microns. When this is substituted into Equation (19.4) along with the values of Z , F and S it gives the value of k .

$$k = 12 \quad (20.2)$$

$$o = 12 D \quad (20.3)$$

This value of k would indicate that the tolerable circle of confusion allowed in measuring the size of a droplet is an order of magnitude larger than the droplet itself. At first this sounds unreasonable. However, it can be attributed to the fact that Equation (19.1) is based on diffused light photography. Although the light used in this work was not collimated, it was kept in a concentrated beam which apparently eliminated a great deal of the scatter evidenced by the tests with the measured beads. A purely collimated beam, of course, would give shadow-graph results with a theoretically infinite depth of field. Nevertheless, Equation (20.1) is very useful in discussing the sampling volume of the camera.

In considering the depth of field of various size droplets relative to the actual spray thickness a maximum droplet size of 200μ will be used. Although in general 200μ cannot be considered the upper limit of all number-size distributions, it is sufficiently greater than the modal values of the distributions which were encountered (see D_{mode} tabulated in Figure 7) to be used as the upper limit of the most significant sections of the distributions.

Thus, if a spray depth is considerably greater than the depth of field of a 200μ droplet (.5" from Equation (20.1)) the data from the photograph can be considered from a thin sampling volume inside the spray and not the entire spray cross section. This is the case at window 3 where the spray depth is approximately two inches.

However, at the first window the average spray is $1/2"$, the same as the 200μ droplet depth of field. At this window all of the droplets

larger than 200μ are considered in focus and will be counted regardless where they are located in the spray, while smaller droplets are counted in only a smaller section of the spray. This is exactly the problem discussed above. It places a very limited value on these distributions such that they should not be used for more than relative studies.

Depth of Field Correction

The result from the droplet size and depth of field study would indicate that the volume used at window 3 in sampling various size droplets was a linear function of the droplet diameters measured. Thus, the counts should be corrected before they are processed to insure that each data point is a count per standard volume.

However, there are four reasons for not using this correction.

The most important is that the depth of field and diameter relationship, Equation (20.1), is at best $\pm 10\%$ accurate. The time needed to properly conduct these tests prohibited more than just a rough result.

Secondly, this correction would increase the count of droplets in the small diameter range more than in the larger diameters. This would tend to make the curves even more skewed to the smaller sizes, crowding them together and thereby increasing the difficulty in distinguishing between them.

Third, the experimental work discussed here was limited to a survey of several variables (see introduction to Section IX) as a guideline to further studies. As such, only comparative distributions were needed. Corrections such as this could be made after the relationship between the depth of field and diameter has been more accurately determined.

Finally, as has been noted above, the correction probably should not be applied to the data from all windows. Since the relationship was no better than 10% accurate, it was not known when to apply the correction and when not to apply it (i.e., correct the data up to what droplet size for the first and second window).

However, before the decision was made to eliminate this correction from the data processing, some of the preliminary data from these tests were corrected in this manner.²

VIII. DATA PROCESSING

This section deals with the methods used in preparing the reduced data (number-size distributions) for the final data analysis. Although this reduced data could be used directly in the data analysis, it would require two subjective judgments.

First, because of the data scatter, a curve would have to be drawn by eye to approximate the distribution. Secondly, these curves would in turn have to be compared visually to be able to detect variations in them as experimental parameters are varied.

Thus, this section explains the attempts which have been made to systematically substitute representative curve distributions for data point distributions. This substitution will allow the objective comparison of the constants of these equations thus avoiding the subjective analysis mentioned above.

Normalization

One of the more significant variables in number size counts is the population density of droplets, or the total number of drops from a given volume of a spray. This variable is usually compared apart from the shapes of the distributions and hence can be eliminated from having an influence on the distributions by dividing all the counts by the total count. Thus, if for each diameter, D_i , the count, n_i , is divided by the total count, $\sum n_i$,^{*} the result, ΔN_i , represents the percent of the total count.

* Three conventions of unmarked summations and integrals are used throughout this work.

$$\sum = \sum_{i=1}^{\ell}$$

$$\int dN = \int_0^1 dN$$

$$\int dD = \int_0^{\infty} dD$$

where ℓ = total number of points in a distribution.

Further, if ΔN_i is defined positively, then N_i represents the percentage of droplets which have diameters equal to or less than D_i .

$$N_i = \sum_{k=1}^i \Delta N_k = \frac{\sum_{k=1}^i n_k}{\sum n_i} \quad (23.1)$$

Some investigators have chosen to define N_i as the percentage of droplets of greater diameters.⁹ This introduces slight differences in their equations compared to those discussed here. Specifically, the N_i used here equals $1 - N_i$ of these other works and ΔN_i here becomes $-\Delta N_i$ in other works.

Some investigators⁹ have attempted to plot the variable $N_i(D)$ rather than $\Delta N_i(D)$ resulting in a monotonically increasing (for positive ΔN_i) "S" curve with the limits of $N(0) = 0$ and $N(\infty) = 1$. However, the physical significance of variations in these curves is a little more obscure than in the ΔN_i plots. Only ΔN_i plots are used in this work.

Standardized Diameter Increments

This normalization corrects only for variations in the size of the sampling of the spray. Different methods of data reduction will still yield different curves. For example, if the data from a count of droplets are grouped into fewer data points than the original data, the count for each point, and hence the percentage of the total count will increase, thereby changing the curve.

If, however, the data is converted to a count per unit diameter increment by dividing the count by the range of diameter, ΔD_i , which each count represents, this problem is eliminated. Then the above regrouping of data into fewer points will give only a less precise representation (assuming scatter is the same) than the original data, rather than an entirely new one.

Thus, the variable which will be used here is:

$$\frac{\Delta N_i}{\Delta D_i} = \frac{\left(\frac{n_i}{\sum n_i} \right)}{\Delta D_i} \quad (23.2)$$

Obviously as the diameter increment, ΔD_i , decreases (and hence the number of diameter groups increases) the function $\frac{\Delta N_i}{\Delta D_i}$ approaches the limit $\frac{dN}{dD}$. Thus, the slope of a N vs. D curve is the value of the $\frac{dN}{dD}$ vs. D curve.

This standard diameter increment allows the data to be regrouped in any desirable way. For instance, counts could be added together and divided by the sum of their ΔD 's to give one new value of $\frac{\Delta N}{\Delta D}$ to replace the original points. Similarly, if desired, a point could be broken into two or more adjacent points (all with $\frac{\Delta N}{\Delta D}$ values equal to the original point, of course) by dividing the count and the ΔD into a set of proportional counts and ΔD 's. A use for such regrouping of points is discussed in the next titled topic.

The reason for using the normalization and standard diameter increment procedures is to allow data from different experiments and/or different data reduction procedures to be compared directly without corrections. Thus, although non-normalized distributions from one test apparatus can be compared directly (assuming uniform data reduction procedures) since the sampling volume is held constant, they cannot be compared with non-normalized distributions from a different apparatus unless the sampling volumes are equal. The normalizing procedure eliminates this variation which occurs between data taken before and after alterations in the apparatus.

Similarly, the distributions obtained from a data reduction procedure which uses a uniform combination of ΔD_i values for all distributions can not be compared to other data which has been reduced by other combinations of ΔD_i . The standard diameter increment corrects this so that all data can be compared regardless of how it was reduced.

Thus, number-size distribution data processed by these two procedures can be compared directly to any other data which have been similarly processed. Such processing eliminates effects of the size of the samples involved or the method of reducing the data from the original form (usually

photographic) to statistical number size form.

Regrouping of Data Points

The need for regrouping of data points (as discussed in the preceding topic) can best be seen by consideration of the implications of relative sizes of ΔD . For example, smaller values of ΔD have both an advantage and a disadvantage. On the positive side, smaller ΔD 's allow more diameters to choose from in measuring a droplet which should give a more accurate distribution.

On the other hand, they also necessitate more diameter groupings which will give fewer counts per diameter group. In experimental work the confidence which is placed in the accuracy of a datum point (whether the inaccuracy is due to statistical or experimental error) is some function of the number of readings made in determining that point. Thus, a point based on one reading has less confidence associated with it than one based on the average of several readings. In number-size distribution work each droplet which is measured can be considered a reading used in evaluating the percentage count in any one photograph of a particular size diameter. Therefore, for a given set of counts, less confidence will be placed on those points in a distribution which is based on a smaller ΔD than on those in a distribution which is based on a larger ΔD because of a lower average count per point.

This problem occurs not only in choosing an overall ΔD value for a number size distribution, but also within any one distribution. A greater confidence can be placed in the points in the larger count regions of a distribution than those in the smaller count regions. Since the curve fitting methods discussed later attempt to pass a curve through all of the points of a distribution without weighting them (i.e., all to be considered equally important and accurate) it is desirable to have a uniform confidence in each point.

One method of obtaining a uniform confidence in the count would be to take advantage of the ΔD regrouping discussed in the preceding topic. By combining small count points into fewer larger points and breaking up very large count points into smaller ones an approximately uniform count could be obtained for all points. The disadvantage of this

method, however, is that the points will be irregularly spaced with more points in the high count than in the low count regions. This will yield a curve which (fitting all points uniformly) will fit the modal regions more closely than the "tails". This would yield data of equal counts and hence equal confidence.

A second method of obtaining equal confidence would be to measure and count droplets of only the low count sizes in additional pictures. This selective counting would be continued until the same count had been obtained for each size. The resulting count per photograph would be obtained by dividing each total count by the number of photographs used to determine it. This would give an evenly spaced set of size increment and data points of equal confidence.

However, this is a rather impractical solution to the problem. The development of additional photographs plus the search through them for droplets of only particular sizes can be quite time consuming. This would only add to the time needed for data reduction which already is the largest stumbling block in obtaining useful data.

Furthermore, care must be taken to insure that all of the photographs used represent identical sprays. Even consecutive photographs from one test run may give data from different parts of a wave of varying droplet population density and size. These waves appear even in sprays under steady-state conditions. As a matter of fact, Section IX will show that this is the most significant variation in number-size droplet distributions encountered in this work.

A final method of using the ΔD in an attempt to handle the data scatter problem is a systematic regrouping of the points into uniformly larger ΔD 's in only certain regions. This would minimize localized scatter problems but again at the expense of creating irregularly spaced points and the resulting curve fitting problem already discussed above. Furthermore, the data points would still be of weighted confidence.

Because each of these correction methods adds a problem for each problem which it eliminates, none of them were used. However, as discussed in Section VII, a regrouping of the ΔD 's was necessary

in the processing of some of the data presented here. This regrouping combined the points into points based on uniformly larger ΔD 's to give a general increase in confidence in all points. This was necessary to eliminate a characteristic in the distributions which was imposed by preferential data reduction procedures. These preferences were shown to avoid the "end" sizes of each successive group of ten diameters (i.e., each successive row of circles on the template). It was assumed that the preferences were symmetrical in each group of 10 sizes and therefore that the points could be combined into two symmetrical and hence non-preferential points. This procedure was applied to distributions 0 to 306 in the following discussion of the data (Section IX). The remaining distributions 310 to 340 were not regrouped since they were counted by using the new procedure which eliminated the preferences (the wedge comparator). But whether the data is uniformly regrouped or presented in its original count form, the data of this work are evenly spaced and of weighted confidence.

Number-Volume Relations

In addition to the number size plots a second popular method of representing droplet distributions is by volume size plots. In such volume plots all droplets are assumed spherical so that the volume of all droplets of a certain size is $n_i \frac{\pi}{6} D_i^3$. Since the volume of fuel is proportional to the energy to be released, the volume size plots have a greater physical meaning than number size plots. However, the D_i^3 correction tends to magnify the absolute value of the data scatter in the large diameter range of a distribution where, because of naturally low counts, the relative data scatter is great (or confidence is small). Because of this scatter problem this work concentrates on number size distribution. If desired, however, subsequent conversion to volume size distribution can be achieved by the following development.

By definition:

$$\Delta N_i \equiv \frac{n_i}{\sum n_i} ; \quad \Delta R_i \equiv \frac{n_i D_i^3}{\sum n_i D_i^3} \quad (27.1)$$

therefore -

$$\Delta N_i = \frac{n_i}{n_i D_i^3} \frac{\sum n_i D_i^3}{\sum n_i} \Delta R_i \quad (28.1)$$

Defining a constant for any given point distribution (consistent with work done in the following topic, Equation (30.5):

$$D_{30} = \left(\frac{\sum n_i D_i^3}{\sum n_i} \right)^{1/3} \quad (28.2)$$

Thus:

$$\Delta N_i = \frac{D_{30}^3}{D_i^3} \Delta R_i \quad (28.3)$$

$$\sum_{k=1}^i \Delta N_k = N_i = D_{30}^3 \sum_{k=1}^i \frac{\Delta R_k}{D_k^3} \quad (28.4)$$

$$\frac{\Delta N_i}{\Delta D_i} = \frac{D_{30}^3}{D_i^3} \frac{\Delta R_i}{\Delta D_i} \quad (28.5)$$

or in continuous form:

$$N = D_{30}^3 \int_0^{\infty} \frac{dR}{D^3} \quad (28.6)$$

$$\frac{dN}{dD} = \frac{D_{30}^3}{D^3} \frac{dR}{dD} \quad (28.7)$$

Notice that to obtain an explicit relation between N and R (or N_i and R_i) a knowledge of $D(D_i)$ as a function of N or R (ΔN_i or ΔR_i) is needed before the integration (summation) can be achieved.

Rather than converting from count data to volume data after a curve has been fitted, it is possible to fit the same equation to both

sets of data resulting in different values of the constants of the equation.

Characteristic Diameters

Often it is desirable to represent a distribution of droplets by a group of droplets of only one simple characteristic size. The value of the characteristic diameter chosen will be a function of those properties of the actual spray which are duplicated in the characteristic spray.

The following actual spray properties are usually considered:

- (1) total number of droplets actually counted, $\sum n_i$ (2) the characteristic length of the spray, $\sum n_i D_i$ (physically this is equivalent to the length of a row of all the droplets in the spray placed end-to-end), (3) the total liquid surface area, $\sum n_i \pi D_i^2$, (4) the total liquid volume, $\sum n_i \rho \frac{\pi}{6} D_i^3$, and (5) what can be called the mass weighted diameter (units of length⁴), $\sum n_i (\rho \frac{\pi}{6} D_i^3) D_i$.

Setting these five properties equal in the real and characteristic spray results in five separate equations. For any distribution (n_i and D_i values known) this gives 5 equations in two unknowns: m , the total number of droplets in the characteristic spray and, D_{vw} , the characteristic diameter.

$$\sum n_i = m \quad (29.1)$$

$$\sum n_i D_i = m D_{vw} \quad (29.2)$$

$$\pi \sum n_i D_i^2 = \pi m D_{vw}^2 \quad (29.3)$$

$$\frac{\rho \pi}{6} \sum n_i D_i^3 = \frac{\rho \pi}{6} m D_{vw}^3 \quad (29.4)$$

$$\frac{\rho \pi}{6} \sum n_i D_i^4 = \frac{\rho \pi}{6} m D_{vw}^4 \quad (29.5)$$

In choosing to equate two of the five properties of the characteristic spray with those properties in the actual spray, two of

the five equations are selected from which the characteristic diameter can be obtained:

$$D_{vw}^{v-w} = \frac{\sum n_i D_i^v}{\sum n_i D_i^w} = \frac{\sum \Delta N_i D_i^v}{\sum \Delta N_i D_i^w} \quad (30.1)$$

In continuous form this becomes:

$$D_{vw}^{v-w} = \lim_{D \rightarrow 0} \frac{\sum \Delta N_i D_i^v}{\sum \Delta N_i D_i^w} = \frac{\int D^v dN}{\int D^w dN} \quad (30.2)$$

The solution of these integrals for various representative curve distributions is discussed in the following topics.

From this it is easier to see how some of the various popular names for these characteristic diameters were obtained.⁵

$$D_{10} = \frac{\sum n_i D_i}{\sum n_i} = \text{number mean, arithmetic mean or average diameter} \quad (30.3)$$

$$D_{20} = \left(\frac{\sum n_i D_i^2}{\sum n_i} \right)^{1/2} = \text{area or surface mean diameter} \quad (30.4)$$

$$D_{30} = \left(\frac{\sum n_i D_i^3}{\sum n_i} \right)^{1/3} = \text{volume mean diameter} \quad (30.5)$$

$$D_{32} = \frac{\sum n_i D_i^3}{\sum n_i D_i^2} = \text{Sauter mean diameter} \quad (30.6)$$

$$D_{43} = \frac{\sum n_i D_i^4}{\sum n_i D_i^3} = \text{mass mean or De Brouckere diameter} \quad (30.7)$$

Since a droplet's volume is proportional to the energy it will release in combustion and evaporation is thought to be proportional to either diameter⁴ or area¹⁰ the D_{31} or D_{32} are perhaps the most significant combustion spray characteristic diameters. However, the D_{30} will

be used in the discussion of the data in Section IX since it was desirable to compare these results with an empirical equation which predicted the D_{30} and not the others.¹¹

There are many other characteristic constants in addition to the diameters which can be defined. In particular there are several which are defined by the probability equations discussed in later topics and which appear as constants in these equations. Although only one of them is used in this work in comparing distributions, all of them are defined in the following development of the curves as an aid to understanding their effect on the curve shapes.

General Comments on Distribution Curves

All of this, however, is only preparatory to the real task of the data processing: replacing the real data point distribution with a representative curve distribution.

All of the equations of the representative curves have the form of a constant times a function of diameter. The constant obviously governs the overall size of the curve. It is not, however, an independent constant to be selected on the basis of a good fit. Just as the variable N_i is defined as a percentage such that $\sum \Delta N_i = 1$, the integral of any curve which is used to represent the counts must also be unity. The value of this constant is determined by satisfying this condition.

Thus, in general:

$$\frac{dN}{dD} = \alpha f(D) \quad (31.1)$$

$$\alpha = \frac{\int dN}{\int f(D) dD} = \frac{1}{\int f(D) dD} \quad (31.2)$$

The constant, α , will be termed the "normalizing constant" and the Equation (31.2), from which it is evaluated will be termed the "normalizing condition".

If all the mass in the photograph is in droplet form, then the normalizing condition must be satisfied. However, if there are ligaments or sheets of water in the photograph, then it may be desirable to make

some attempt to correct for this in order to insure that the percentage of droplets is taken relative to the total mass in the photograph. This approach will shed light on how much of the injected fuel has been formed into droplets which may have an effect on the burning rate distribution.

Since this is a mass measurement, such a correction could be made more easily in a $\frac{dR}{dD}$ equation. If a systematic method of making this correction can be established this would be an excellent reason for using R as the droplet count variable rather than N .

However, setting up such a correction procedure appears to be a formidable problem. Not only are the ligaments of irregular shapes and therefore not conducive to volumetric measurements, but also, their boundaries are obscured by other ligaments. The problem is further complicated by the depth of field of the camera which causes parts of the ligaments' boundaries to be out of focus. Therefore, comments in the following discussion of the data are limited to very general quantitative estimates made by eye from the photographs and hence are mentioned only in the extreme cases of very few ligaments or very few droplets.

Evaluating the Successfulness of a Curve Representation

The solution of Equation (30.2) for both the original data point distribution and the representative curve distribution characteristic diameters can be used to evaluate how well a curve represents the physical properties of the actual spray.

Notice that the Equation (31.1) (or similar point distribution data) allows Equation (30.2) (or Equation (30.1)) to be solved, if only by numerical integrations. Thus, the most generalized form of a characteristic diameter of a curve distribution is (Equation (31.1) substituted into Equation (30.2)):

$$D_{vw}^{v-w} = \frac{\int D^v f(D) dD}{\int D^w f(D) dD} \quad (32.1)$$

In the equations to be discussed, only one case can be integrated to give an explicit relationship between the generalized characteristic diameter and a constant of the equation for the curve. In all other cases

Equation (32.1) gives two non-analytic integrals necessitating numerical integrations.

A more direct way of evaluating how well a curve represents a point distribution is a measure of the "fit" of the curve. This is the sum, ϵ , of the graphical area between the curve and the data points. It is a measure of how closely the curve comes to passing through each data point.

$$\epsilon \equiv \sum \left| \frac{\Delta N_i}{\Delta D_i} - \alpha f(D_i) \right| \Delta D_i \quad (33.1)$$

Since by definition

$$\sum \frac{\Delta N_i}{\Delta D_i} \Delta D_i = 1 \quad (33.2)$$

and furthermore, the numerical integration of Equation (31.2) gives:

$$\alpha \int f(D) dD = \sum \alpha f(D_i) \Delta D_i = 1 \quad (33.3)$$

the value of ϵ can have a maximum value of 2. However, for any well fitting curve ϵ can be expected to be some fraction of 1 and hence can be expressed as a percentage. Thus, a value of .24 or 24% for ϵ indicates that the area between the data points and the curve is about 1/4 of the area under either the point or curve distribution. Or in other words, 12% of the area under the point distribution must be "removed" and "reshaped" before it is "added" back to form the smoother curve distribution. Because of the absolute value which must be taken in evaluating ϵ , it is difficult to handle Equation (33.1) analytically. Thus when an error function is needed that can be analytically minimized the square error, E , is used:

$$E \equiv \sum \left(\frac{\Delta N_i}{\Delta D_i} - \alpha f(D_i) \right)^2 \quad (33.4)$$

It, however, also has a shortcoming for its value is a function of the number of data points considered.

Thus, since E makes possible an analytical analysis of the curve fitting error at the expense of wide ranges of values, it is used only in finding the proper fit for each curve, whether by iterative or trial-and-error methods. Conversely, since ϵ is difficult to treat analytically but gives consistently comparative values of the error of all the fits, it was used to evaluate the "fit" of the curves once the error, E , had been minimized.

The Distribution Curves

Because of the natural "cocked hat" shape of typical distribution data, the most logical curves to use in representing the data are variations of negative exponentials. These give an appropriately shaped "tail" in the large diameter end of the curve. However, pure negative exponentials also have an unrealistic finite count at zero diameter so must be corrected to give a second tail at the smaller diameter end. This second tail must end with a zero value at zero diameter. The nature of the corrections made to achieve this constitute the two basic forms of curves used.

The first of these is to use a probability approach. In this the exponent is made to have symmetrical negative values about a mean diameter thereby giving two "tails". This was first used in spray studies by Hatch and Choate in 1929.⁶

The second method was introduced in 1938 by Nukiyama and Tanasawa and has come to bear their names.¹ In this method the negative exponential is multiplied by a diameter term raised to a power which, of course, is zero at zero diameter.

Probability Equations

The conventional form of the probability equation is:⁶

$$\frac{dN}{dD} = a e^{-(D-D_{10})^2 / 2\sigma^2} \quad (34.1)$$

where: D_{10} = arithmetic mean (defined earlier) (34.2)

$$\sigma^2 = \text{standard (or average) deviation} = \int (D-D_{10})^2 dN = \sum (D_i-D_{10})^2 \Delta N_i \quad (35.1)$$

The normalizing constant, a , can be evaluated from the normalizing condition yielding:

$$a = \frac{1}{\sigma \sqrt{2\pi}} \quad (35.2)$$

This equation, however, predicts non-zero counts of droplets not only to infinite sizes, but more importantly to negative sizes. This negative range can be corrected by using the variable $\ln D$ to replace D (and hence $\ln M$ for D_{10}) resulting in the "log probability equation":

$$\frac{dN}{dD} = b e^{-\left(\ln \frac{D}{M}\right)^2 / 2(\ln \sigma)^2} \quad (35.3)$$

where:

$$\ln M = \int \ln D dN = \sum (\ln D_i) \Delta N_i \quad (35.4)$$

$$(\ln \sigma)^2 = \int \left(\ln \frac{D}{M}\right)^2 dN = \sum \left(\ln \frac{D_i}{M}\right)^2 \Delta N_i \quad (35.5)$$

The evaluation of b follows from the normalizing condition:

$$b = \frac{1}{\int_0^{+\infty} e^{-\left(\ln \frac{D}{M}\right)^2 / 2(\ln \sigma)^2} dD} \quad (35.6)$$

However, this can be solved only by numerical means.

The prediction of non-zero counts of droplets to $+\infty$ sizes still exists. It can be corrected by use of the "upper limit probability equation" which was introduced by Mugele and Evans.⁵

$$\frac{dN}{dD} = c e^{-\left(\ln \frac{D^s}{D_M^s - D^s}\right)^2 / 2(\ln \gamma)^2} \quad (36.1)$$

In this form the concept of a mean diameter is replaced by that of a maximum diameter, D_M . For sizes larger than this maximum diameter the curve predicts imaginary values, which are interpreted as zero counts. Mugele and Evans have suggested that this maximum diameter is the size of droplets created by the injector orifices and from which the spray break up mechanisms create all the smaller size droplets.

The constant, $\ln \gamma$, is an average value of the new deviation function, $\left(\ln \frac{D^s}{D_M^s - D^s}\right)^2$, and so can be termed an "average deviation"

The substitution of this new deviation term for the $(D - D_{10})^2$ term in Equation (35.1) supports this:

$$(\ln \gamma)^2 = \int \left(\ln \frac{D^s}{D_M^s - D^s}\right)^2 dN = \sum \left(\ln \frac{D_i^s}{D_M^s - D_i^s}\right)^2 \Delta N_i \quad (36.2)$$

The choice of values for the parameter s implies apriori certain curve shapes. The nature of this influence is seen by considering the maximum value (modal point) on the curve. This will occur at:

$$-\left(\ln \frac{D_{mode}^s}{D_M^s - D_{mode}^s}\right)^2 = 0 \quad (36.3)$$

solving for D_{mode} :

$$D_{mode} = \frac{D_M}{2^{1/s}} \quad (36.4)$$

$$\text{thus for:} \quad s < 1 \quad D_{\text{mode}} < \frac{D_M}{2} \quad (37.1)$$

$$s = 1 \quad D_{\text{mode}} = \frac{D_M}{2} \quad (37.2)$$

$$s > 1 \quad D_{\text{mode}} > \frac{D_M}{2} \quad (37.3)$$

Clearly, since the values of s recommended by Mugele and Evans were all ≥ 1 ($s = 1, 2, 3$), they had limited themselves to curves skewed to the large diameter end.

Thus, rather than using only the values recommended by Mugele and Evans, a variety of values $>$ and < 1 have been chosen. Since $s = 1, 2, 3$ correspond respectively to a D_{mode} of $.5, .7$ and $.8 D_M$, the additional values of s were chosen to give a complete spectrum of skewed curves such that D_{mode} assumed values approximately equal to multiples of $.1 D_M$ from $.1 D_M$ to $.9 D_M$. This corresponds to $s = \frac{3}{10}, \frac{4}{9}, \frac{5}{9}, \frac{3}{4}, 1, 1 \frac{1}{3}, 2, 3, 6 \frac{1}{2}$.

Again the constant c can be evaluated only numerically:

$$c = \frac{1}{\int_0^{D_M} e^{-\left(\ln \frac{D^s}{D_M^s - D^s}\right)^2 / 2(\ln \gamma)^2} dD} \quad (37.4)$$

The log and upper-limit probability equations are the only probability equations in this work.

Nukiyama-Tanasawa Equation

The most general form of the Nukiyama-Tanasawa equation¹ is:

$$\frac{dN}{dD} = A D^p e^{-CD^q} \quad (37.5)$$

Here p and q are parameters.

If they are chosen such that:

$$p = q - 4 \quad (38.1)$$

the resulting special case is known as the Rosin-Rammer distribution.⁹

The constant C can be related to any of the characteristic diameters explained earlier through Equation (32.1). For the Nukiyama-Tanasawa Equation this becomes:

$$(D_{vw})^{v-w} = \frac{\int D^{v+p} e^{-CD^q} dD}{\int D^{w+p} e^{-CD^q} dD} \quad (38.2)$$

Defining:

$$y = CD^q \quad (38.3)$$

$$(D_{vw})^{v-w} = \left(C^{-\frac{1}{q}} \right)^{v-w} \frac{\int_0^\infty y^{\frac{p+1+v}{q} - 1} e^{-y} dy}{\int_0^\infty y^{\frac{p+1+w}{q} - 1} e^{-y} dy} \quad (38.4)$$

The two integrals are recognized as gamma functions. Thus:

$$C = \frac{1}{(D_{vw})^q} \left(\frac{\sqrt{\frac{p+1+v}{q}}}{\sqrt{\frac{p+1+w}{q}}} \right)^{\frac{q}{v-w}} \quad (38.5)$$

Since p and q are equation parameters while v and w are arbitrary, C can be expressed solely as a function of any characteristic diameter.

The constant A can be evaluated analytically from the normalizing condition:

$$A = C \frac{\frac{p+1}{q}}{\sqrt{\frac{p+1}{q}}} q \quad (38.6)$$

Linear Curve Fits

Each of these equations can be transformed into a linear form in which there are two constants that are determined by the slope and intercept of the curve. All other unknowns in the equations can be treated as parameters. Thus, after the transforming equations are applied, the equations are of the form:

$$Y = G X + B \quad (39.1)$$

The linearized form of the log probability Equation (35.3) is:

$$\ln \frac{dN}{dD} = \ln b - \frac{1}{2(\ln \sigma)^2} \left(\ln \frac{D}{M} \right)^2 \quad (39.2)$$

$$\text{With } X = \left(\ln \frac{D}{M} \right)^2 \quad (39.3)$$

$$Y = \ln \frac{dN}{dD} \quad (39.4)$$

$$G = \frac{1}{2(\ln \sigma)^2} \quad (39.5)$$

$$B = \ln b \quad (39.6)$$

It is apparent that after fitting the curve, the slope and intercept give values of σ and b instead of M and σ which are the independent constants (b being dependent upon them through the normalizing condition, Equation (35.6)). M must be known before the values of X_i can be obtained. Thus, a trial-and-error solution for b , M and σ is needed.

A value for M is assigned (the D_{10} of the actual data points would seem appropriate as a first guess) and the curve fitted to give values of b and σ from the intercept and slope respectively. A second value of b which satisfies the normalizing condition can then be determined from M and σ by a numerical integration of Equation (35.6). The comparison of these two values of b will lead to a new value for M . This process is repeated until the two b values are

within an acceptable error.

The same procedure will be used on the upper limit probability Equation (35.1) in its linear form:

$$\ln \frac{dN}{dD} = \ln c - \frac{1}{2(\ln \gamma)^2} \left(\ln \frac{D^s}{D_M^s - D^s} \right)^2 \quad (40.1)$$

with

$$X = \left(\ln \frac{D^s}{D_M^s - D^s} \right)^2 \quad (40.2)$$

$$Y = \ln \frac{dN}{dD} \quad (40.3)$$

$$G = \frac{1}{2(\ln \gamma)^2} \quad (40.4)$$

$$B = \ln c \quad (40.5)$$

where now c must also satisfy the normalizing condition Equation (37.4). In this case D_M is varied until the intercept gives a value of c which agrees with Equation (37.4).

In the Nukiyama-Tanasawa Equation, however, there is only one independent constant, C . Thus, if A is to satisfy the normalization condition, Equation (38.6), one or both of the parameters, p or q , will have to be treated as a curve fitting constant similar to the procedure used in the probability fit. This is contrary to the philosophy of p and q . These were intended to be parameters which are multiples of $1/2$. Other investigators¹² have chosen to keep p and q as parameters and disregard the normalization condition.

Thus, the linear form of Equation (37.5) is:

$$\ln \frac{dN}{dD} \frac{1}{D^p} = \ln A - CD^q \quad (40.6)$$

$$X = D^q \quad (40.7)$$

$$Y = \ln \left(\frac{dN}{dD} \frac{1}{D^p} \right) \quad (41.1)$$

$$G = -C \quad (41.2)$$

$$B = \ln A \quad (41.3)$$

In contrast to the probability equations this linear method leads to a direct solution. Once the parameters p and q are assigned values Equation (41.2) and Equation (41.3) give exact values for C and A . Remember, however, that this is at the expense of a normalized A .

Attempt to Use Least Square Linear Fit

It seems most natural at this point to apply the square error minimization to obtain a least square error fit. If Equation (39.3), (40.2), or (40.7) is used to find values of X_i for every D_i , then values for Y_i' can be obtained from Equation (39.1) as points of the linearized curve. Similarly, if the substitution of $\frac{dN}{dD} = \frac{\Delta N}{\Delta D}$ is used in Equation (39.4), (40.3) or (41.1) values of Y_i can be found as real data points in the linearized set of coordinates. The difference between the curve points, Y_i' , and the data points, Y_i , can be put into a square error equation as in Equation (33.4) :

$$E = \sum (Y_i' - Y_i)^2 = \sum (GX_i + B - Y_i)^2 \quad (41.4)$$

Again, X_i and Y_i are found from Equations (39.3) and (39.4), (40.2) and (40.3) or (40.7) and (41.1) respectively (depending on the distribution curve used). This error can be minimized relative to the slope, G , and the intercept, B , and then solved for these two variables to give:

$$B = \frac{\sum X_i \sum X_i Y_i - \sum Y_i \sum X_i^2}{(\sum X_i)^2 - 2 \sum X_i} \quad (41.5)$$

$$G = \frac{\sum Y_i - l_B}{\sum X_i} \quad (42.1)$$

In spite of the simplicity of this result it is far from satisfactory for several reasons. Since it is an unsatisfactory method it may seem fruitless to discuss these reasons. However, they provide a convenient background for understanding the methods of curve fitting which were finally selected.

Because of the cocked hat shape of these curves, the linearizing transformations must necessarily magnify the large diameter end of the curve much more than in the modal region. As a result, the error terms, $(Y_i' - Y_i)$, used in the linear fits are considerably weighted if they are converted to the nonlinear coordinates through the reverse transformation. This results in a curve which is fitted more closely to the large diameter end of the data than to the modal region and small diameter end of the data. This can be avoided somewhat by combining data in the large diameter region into fewer data points with larger ΔD_i as discussed in the "Standardized Diameter Increments" section.

Furthermore, the use of the linear least square error technique involves a minimization relative to the slope and intercept. To be an accurate minimization these should correspond to the two independent constants of the curves. However, in each case the intercept is a function only of the dependent constant (the normalizing constant) so that the error is not properly minimized. This problem cannot be avoided if the linear fit were to be used on the Nukiyama-Tanasawa Equation because there is only one independent constant.

In contrast to the above, both probability equations do have a second independent constant. Therefore, minimizing the error relative to one independent constant (through the slope) and one dependent constant (through the intercept) does not give the same result as minimizing it relative to two independent constants. For example, in the linear fit of the log probability equation the total square error, E , is minimized

by solving:

$$\frac{\partial E(\sigma, M, b)}{\partial \sigma} = 0 \quad (43.1)$$

$$\frac{\partial E(\sigma, M, b)}{\partial b} = 0 \quad (43.2)$$

instead of:

$$\frac{\partial E(\sigma, M)}{\partial \sigma} = \frac{\partial E(\sigma, M, b)}{\partial \sigma} + \frac{\partial E(\sigma, M, b)}{\partial b} \frac{\partial b(\sigma, M)}{\partial \sigma} = 0 \quad (43.3)$$

$$\frac{\partial E(\sigma, M)}{\partial M} = \frac{\partial E(\sigma, M, b)}{\partial M} + \frac{\partial E(\sigma, M, b)}{\partial b} \frac{\partial b(\sigma, M)}{\partial M} = 0 \quad (43.4)$$

where $b(\sigma, M)$ is the normalizing condition and $E(\sigma, M)$ is the total square error after b is replaced by $b(\sigma, M)$. This incorrect minimization cannot be avoided in the linear case without losing the comparative simplicity of Equations (41.5) and (42.1).

The large diameter weighting and/or the incorrect minimization are probably the reasons why the least-square error method has not been used by others with the linearization technique. Thus, only a subjective "eye ball" fit can be used while still preserving the simplicity of the linearization concept. In addition to being subjective this also ignores the normalizing condition.

Nonlinear Least Square Curve Fit

A least square error fitting technique in the real (non-linear) $\frac{dN}{dD}$ vs. D coordinate system was used to avoid the weighted error problem. Furthermore, in this new technique, Equations (43.3) and (43.4) were considered in minimizing the probability error. Finally, proper consideration was given in this nonlinear method to the normalizing condition in all equations.

In the log probability equation, the square error is:

$$E = \sum \left(\frac{\Delta N_i}{\Delta D} - b e^{-\left(\ln \frac{D_i}{M} \right)^2 / 2(\ln \sigma)^2} \right)^2 \quad (43.5)$$

Three partial derivatives of this (relative to σ , M and b) and two of the normalizing conditions in Equation (35.6) (relative to σ and M) are needed to be able to evaluate Equations (43.3) and (43.4). Since Equation (35.6) can be evaluated only by numerical methods, the $\frac{\partial b}{\partial \sigma}$ and $\frac{\partial b}{\partial M}$ terms in Equations (49.3) and (43.4) will also require numerical solutions. The solution for the three unknowns, σ , M and b, involves a double trial and error solution on three Equations, (35.6), (43.3) and (43.4) all of which contain numerical integrations and two of which contain several series of up to 50 terms (in the case of the data presented in this work). Even the most simple attempts to iterate to the solution will be quite involved. Obviously, the solution must be handled by a computer. But rather than becoming involved in this complexity it is simpler just to use a trial and error method of minimizing E directly, rather than finding the roots of its derivatives. Thus, by guessing values of M and σ , b can be evaluated from Equation (35.6) and E from Equation (43.5). Successive trials will lead to the minimum value of E, the best fit. This also has the advantage of yielding a true minimum, whereas the solution of Equations (35.6), (43.3) and (43.4) does not exclude the possibility of locating a saddle point (or local minimum) in the E(σ , M) function.

Exactly the same conclusions are reached concerning the upper-limit probability curve, again because of the numerical integration form of the normalizing condition, Equation (37.4) and the presence of two constants.

In the Nukiyama-Tanasawa Equation, however, the total square error is given by:

$$E = \sum \left(\frac{\Delta N_i}{\Delta D_i} - A D^p e^{-CD^q} \right)^2 \quad (44.1)$$

Since there is only one independent constant this is more easily minimized than the probability equations:

$$\frac{dE}{dC} = 2 \sum (A f_i - W_i) \left(A \frac{df_i}{dC} + \frac{dA}{dC} f_i \right) = 0 \quad (44.2)$$

where:

$$f_i = f(D_i) \equiv D_i^p e^{-CD_i^q} \quad (45.1)$$

$$\frac{df_i}{dC} = -D_i^q f_i \quad (45.2)$$

$$W_i \equiv \frac{N_i}{D_i} \quad (45.3)$$

$$A = \frac{q C^{\frac{p+1}{q}}}{\sqrt{\frac{p+1}{q}}} \quad (45.4)$$

$$\frac{dA}{dC} = \frac{p+1}{Cq} A \quad (45.5)$$

C cannot be found explicitly, so again a trial and error solution is necessary. The Newton-Raphson method is useful in finding the roots of Equation (44.2). Thus:

$$C_{\text{new}} = C_{\text{old}} - \frac{\frac{dE}{dC}}{\frac{d^2E}{dC^2}} \quad (45.6)$$

where:

$$\frac{d^2E}{dC^2} = 2 \sum \left((A f_i - W_i) \left(A \frac{d^2 f_i}{dC^2} + 2 \frac{dA}{dC} \frac{df_i}{dC} + \frac{d^2 A}{dC^2} X_i^2 \right) + \left(A \frac{df_i}{dC} + \frac{dA}{dC} f_i \right)^2 \right) \quad (45.7)$$

$$\frac{d^2 f_i}{dC^2} = -D_i^q \frac{df_i}{dC} \quad (45.8)$$

$$\frac{d^2 A}{dC^2} = \frac{dA}{dC} \frac{1}{C} \frac{p+1}{q} - 1 \quad (45.9)$$

Multimodal Distributions

Some investigators have indicated bimodal fuel drop size distributions.¹³ Clearly, such tendencies cannot be manifested in curves of the nature discussed. Although more sophisticated curves may be formulated and fitted to the data there are two immediate possibilities which might be more meaningful than totally new equations. The first would be the addition of two equations of any one of the forms discussed. This is more than twice as involved numerically as a simple modal curve fit since the two normalizing constants need to satisfy only one combined normalizing condition. This effectively leaves one of these two constants as an additional independent constant which can be used to obtain a good fit. Thus there are $2 \frac{1}{2}$ times more independent constants in the bimodal curve than there are in the single modal curve. In the probability curves this means there will be 5 constants to be selected by trial and error while in the Nukiyama-Tanasawa Equation a choice of three values for the parameter p and three for q would yield 81 different combinations of curves from which to choose the best fit.

A second method would be to superimpose a power series curve on the modal section of a distribution. This would have to be done such that the variation between the power series curve and the original curve integrates to zero, thereby maintaining the normalizing condition. Though perhaps simpler, this method would produce constants which would lack any physical significance.

IX. RESULTS AND CONCLUSIONS

This section deals with the selection of the best fitting curve to represent the point distributions and the results obtained from comparing these curve distributions once fitted to the experimental data.

The effects of five different experimental parameters or operating conditions have been studied using the still camera to determine spray drop size distributions. For all the tests the chamber length was 13" and the associated frequency of pressure oscillation 530 cps. The standard test condition involved: 1), a chamber pressure (P_c) of 100 psig; 2), a 50 psia injector pressure drop (ΔP); 3), the .040" diameter doublet injector; 4), all photographs were taken 3 3/4" downstream from the injector, x . The five studies were directed at variations in each of these 4 parameters plus a comparison of the steady-state to oscillating pressure conditions. The oscillating pressure studies were made on nearly all the other operating conditions and not just the standard condition.

Computer programs were completed which fit the Nukiyama-Tanasawa Equations to the data by the iterative method and the two probability equations by the trial and error methods discussed in the previous section.

Best Fitting Curve

The results of fitting the curves to the data showed little difference between any of the curves. The log probability equation provided the best fit in 16½ of the 35 cases, the Nukiyama-Tanasawa curve was best in 10 and the upper-limit probability curve provided the best fit in the remaining 8½. A summary of the graphical area error, ϵ , for each distribution is listed in Figure 5. In many cases, the differences between the best fit and the other curves was not significant so that almost any one of the conditions could have been used successfully. Thus, other criteria for choosing the best curve had to be used.

In the Nukiyama-Tanasawa Equation, no consistent parameter preferences were indicated for either p or q as can be seen in Figure 5. This means that three values (one constant, C , and two parameters, p and q) must be stated to completely describe any distribution by this equation.

This was expected since the Nukiyama-Tanasawa Equation has only one curve fitting constant, C . Thus, to have the same versatility in fitting the data as either of the two constant probability equations, the best Nukiyama-Tanasawa fit had to be chosen from a variety of combinations of the parameters. Furthermore, the constants and parameters in the probability equations have simple physical meanings in terms of the shape of their curves while the meaning of the constant and particularly the parameters in the Nukiyama-Tanasawa Equation are somewhat obscured. For these reasons, and based on the evidence that the Nukiyama-Tanasawa Equation does not in general fit the data any better than the probability equations, it was discarded.

A conclusive choice between the log and upper-limit probability equations was based on the success of reproducing the physical properties of the actual spray. In particular, the volume mean diameter, D_{30} , was studied. By comparing the D_{30} from the two curves (see Equation (32.1)) to the actual value, Equation (30.5), it was found that the upper-limit probability equation succeeded in duplicating it much more accurately than the log probability equation. The results of this are also shown in Figure 5. The reason for this is that the log probability equation predicts counts of droplets to infinite sizes. Because the volume is proportional to the cube of the diameter, these larger diameters are weighted more heavily than the smaller diameters in evaluating the D_{30} , resulting in a value closer to these unrealistic diameters, i.e., a larger value. It is for this reason that the upper-limit probability equation was chosen for these studies.

Interpreting the Upper-Limit Curves

Although the value of $s = 3/10$ gave the best upper-limit fits in nearly half (16 out of 35) of the distributions, values of $s = 4/9$, $5/9$ and $3/4$ also gave best fits (in 6, 5, and 8 cases respectively). Thus, where the values of two constants completely describe the log probability curve, the value of an additional parameter is needed for the upper-limit curve. This extra parameter can be eliminated, however, by use of Equation (36.4).

It is interesting to note from this parameter preference data, that in not one case did the originally recommended values of s provide the best fit ($s = 1, 2, 3$). Furthermore, the great preference for the

smallest value of s , $3/10$, would seem to indicate that even smaller values would, in some cases, provide better fits. This was evident in several of the distributions after the curves were fitted to the data. In Figure 9, for example, distribution #130 would have a better fitting curve if the tail were made longer. If this were done by increasing D_M without changing the value of D_{mode} the overall shape of the curve would be more skewed to the left than the one shown. This would require a lower value of s than the $3/10$ used there.

This condition would have been even more evident if the linear depth of field correction discussed in Section VII had been used. In future work, (which should include a correction similar to that discussed), it is recommended that values of s should be chosen to allow D_{mode} to cover the range from $.01$ to $.5 D_M$ ($s = \frac{3}{20}$ to 1) in intervals such that most of these locations are in the $.01$ to $.2 D_M$ region ($s = \frac{3}{20}$ to $\frac{4}{9}$).

The method used in analyzing the data was to plot all the constants of the curves and then look for trends in the plots. All 35 distributions are shown this way in Figure 6. A list of operating conditions and values of the constants for the best upper-limit fit are given for each distribution in Figure 7. In the following discussion on the distribution characteristics it will be helpful for the reader to note the tendencies in these plots in addition to observing the physical changes in the individual distribution shapes.

Droplet Wave Phenomenon

The only trend that could be found in the data was related to droplet population densities in the photographs. For instance, distributions 130 and 240 were taken under identical conditions and yet have distributions which differ primarily by their modal values (Figure 9). The only difference in spray conditions which could be found to explain this and other similar distribution differences was the total number of droplets counted for the same spray area in each case. Distribution 130 has a comparatively low count (1154) and has a curve with modal value at 38μ while distribution 240 has a high count (2525) and a curve with somewhat similar shape but with a modal value of 107μ . This result was found in the $.040''$, $.059''$ and pair of $.059''$ injectors.

The .170" injector also displayed variations in distributions which were dependent on the wave phenomenon. However, these variations were of a slightly different nature. For the .170" injector the low count distributions had a very blunt peak at a somewhat larger modal value than the high count distributions (see distributions 70 and 80 respectively in Figure 8) while for the other injectors the low count distributions had shapes similar to the high count but of smaller modal values.

The .120" injector had variations in its distributions similar to those in the smaller injectors. However, these could not be attributed to the population density waves.

Thus, the .120" injector seems to provide a transition from the .170" type of wave distributions to the smaller injector results, indicating that it has a less cyclic drop size distribution scatter throughout its spray.

However, the results from the .120" injector and especially the .170" injector are doubtful for several reasons. First, only part of the total injected mass had been formed into droplets at the location at which the data were taken. Furthermore, because of the great flow of liquid through this injector the spray was quite dense, hard to photograph and consequently difficult to reduce to drop size data. This presented such a problem in the .170" injector tests that the pressure drop across it (and hence the jet velocity and the mass flow rate) had to be lowered to 10 psi from the standard 50 psi in order to get these photographs. Finally, the counts in these distributions were some of the lowest recorded. Thus, because of the lower photographic quality and the low counts these .120" and .170" injector distributions are presented with much less confidence than the others. Further, even if this tendency for the .170" injector is assumed to really exist, it is not clear from the present data if this change in high-low count distributions results from 1) larger injector sizes, 2) a spray zone of low-droplet, high-ligament densities or 3) a lower jet velocity (in the .170" case).

This variation in droplet population density was investigated further by the streak camera discussed earlier. Tests using this camera were conducted only on the standard condition. Figure 9 shows a very prominent

cyclic variation in the number of droplets recorded passing the test section. The frequencies observed were around 100 cps or about $1/5$ of the natural frequency of the chamber. At times this variation became as great as 3 to 1 in relative magnitude.

These waves were unaffected by longitudinal acoustic waves which were established by the siren exhaust. This appears to be in conflict with other¹⁴ results which show a coupling between such waves and pressure oscillations. However, this other work involved oscillations of up to 30% of the mean pressure which is much greater than the 5% induced for this data. Further, the impinging jet droplet waves in this other work were attributed to interactions between the pressure and the fuel jets before impingement. Such an interaction is not possible with the design of the injectors used here (Figure 4) in which impingement occurs at the injector face.

A precise measurement of these frequencies could not be obtained without rebuilding the streak camera to give longer exposures. However, working with a frequency of 100 cps and an average droplet velocity at this location of 30 ft/sec., each cycle is about $3\frac{1}{2}$ " long within the spray. Since the photographic test section is only $1/2$ " wide it is clear that variations in droplet counts of 3 to 1 should be expected from the distribution photographs.

This periodic irregularity is, of course, of immediate interest to combustion instability. The important points to note are that the frequency observed is about $1/5$ of the natural acoustic longitudinal frequency of the chamber and that this phenomena seems to be unaffected by setting up such higher frequency oscillations. This clearly indicates that it is not a result of a resonant mechanism between the chamber acoustic properties and the spray.

Consider the physical significance of waves of different number-size distributions on a rocket. The different distributions would be expected to burn with different characteristics (as discussed in Section V) so would probably form some cyclic combustion pattern. This would, of course, be particularly harmful when in the case where the combustion would be in resonance with an acoustic frequency of the chamber. Combustion-acoustic interaction effects are precisely what the research in combustion instability is attempting to discover and understand with an aim at eliminating or minimizing such effects.

Longitudinal Resonant Pressure Oscillations

The lack of consistent changes in spray characteristics between steady-state and oscillating pressure tests was seen in all the drop size distribution results. This can be seen by comparing distributions 140 and 160 (Figure 8) which represent steady-state and oscillating pressure conditions, respectively, and yet are nearly identical. Variations which were found were all attributable to the wave population density phenomena or data scatter.

These results would therefore substantiate the assumption made by Strahle and Crocco¹⁵ that longitudinal mode pressure oscillations in the range of rocket motor noise is not sufficient to trigger linear instabilities through an injector spray characteristic coupling mechanism even under resonant conditions.

Longitudinal Locations

By taking data at three points longitudinally from the injector under the standard operating conditions it was hoped that variations in droplet size distributions as the ligaments break up into droplets could be seen and possibly be related to the .120" and .170" injector wave results.

No differences were found in these distributions except for the population density wave effects already mentioned. Presumably this lack of differences is due to the comparatively fast breakup of the .040" injector ligaments into droplets. While the .040" injector exhibited nearly immediate (within 1/2") formation of droplets, over half of the injected mass from the .170" injector was still in ligament form as far as 3 3/4" downstream of the injector. Because of this difference a direct comparison of breakup data cannot be made between the .040" and the .120" and .170" injectors.

Furthermore, as discussed earlier (Section VII), the data taken from the closer windows are rather limited in their usefulness since a precise definition of the sampling volume could not be made.

Injector Pressure Drop

A series of tests was run using a higher pressure drop in an otherwise standard testing condition. The greater mass flow rate made photographing the spray more difficult and ligaments were found to extend

further downstream than under the standard pressure drop. This extension of ligament locations is in agreement with other work.⁷ However, no significant change was found in the drop size distributions.

Chamber Pressure

The final series of tests compared distributions at lower chamber pressures to the standard pressure. The results of these data showed two points. First, there is no difference between the lower and higher pressure runs as far as drop size distributions are concerned. Secondly, the droplet population phenomena appeared to have disappeared at lower pressures. This second result was expected since the waves of droplets should approach the range of 2000 to 3000 cps as reported in earlier works performed at a pressure of one atmosphere.¹⁶ Thus, several cycles should be included in each photograph averaging out any cyclic variations in distributions. The fact that a high and low count did exist (distributions 330 and 340 respectively) can be attributed to the accidental over development of the negatives used for the low count distribution. This appears to have "washed out" many of the droplets which were slightly out of focus, but still capable of being measured. To verify this a count (without measurements) was made of droplets in all negatives developed in each group. Those in the overdeveloped group averaged 57% fewer counts than in the normal development group while the largest underdeveloped count was 80% of the lowest normal development count. Furthermore, the high and low counts in each group were at worst in a ratio of slightly less than 3 to 2 rather than 3 to 1 as experienced for the wave phenomena. Finally, in spite of this difference nearly identical distribution curves were obtained from these two photographs.

Since several cycles are included in each low chamber pressure photograph and since the high and low chamber pressure distributions were similar, it is not surprising to find that the distributions show characteristics which are similar to the curve resulting from adding a high and a low count distribution together. This is seen in Figure 9 where distributions 130 and 240 have been added together to give distribution 137 which compares favorably with distribution 330.

Thus, it seems that the droplet population density waves which have been studied in atmospheric pressures¹⁶ are lower in frequency when measured under high pressures. More specifically, for an order of magnitude

increase in pressure there is an order of magnitude decrease in frequency. If this frequency-chamber pressure relationship is a continuous one, it may have a very definite significance for certain cases of combustion instability, again especially when the droplet population frequency for a certain chamber pressure is in resonance with the natural chamber acoustic frequency. Even in the case where such coupling is not present, droplet population density variations may explain certain buzz-type* phenomena, i.e., low amplitude non-acoustic oscillations characteristically nondestructive although often responsible for performance losses.

Prediction of D_{30}

An equation for the prediction of D_{30} values has been derived empirically by Ingebo¹¹:

$$\frac{D_j}{D_{30}} = 2.64 D_j V_j + .97 D_j \Delta V \quad (54.1)$$

where D_j is the impinging jet diameter, V_j its velocity and ΔV the velocity difference between the background gas stream and the liquid jet.

Because of the side injection of the nitrogen the evaluation of ΔV is somewhat difficult for the test apparatus used. This undoubtedly accounts for a large part of the differences between the Ingebo predicted D_{30} and the curve fitted D_{30} as shown in Figure 5. A sufficient number of distributions do agree with the Ingebo equation to indicate that the equation can be used to predict characteristic diameters of sprays produced in more dense gases than those in which the original tests were conducted. Notice in Table 5, however, that the 4 worst agreements between the D_{30} 's were for the .170" injector where ligaments predominate in the photographs. This suggests that the Ingebo equation can be used only in fully-developed sprays or, again, that the data is not too trustworthy for this injector.

Concluding Remarks

All of these results are admittedly based on rather limited data samples. First, there were only a few distributions for each condition. Furthermore, each distribution was based on rather low total counts resulting

* Frequencies for the buzz-type oscillations fall between chugging and acoustic type instabilities.

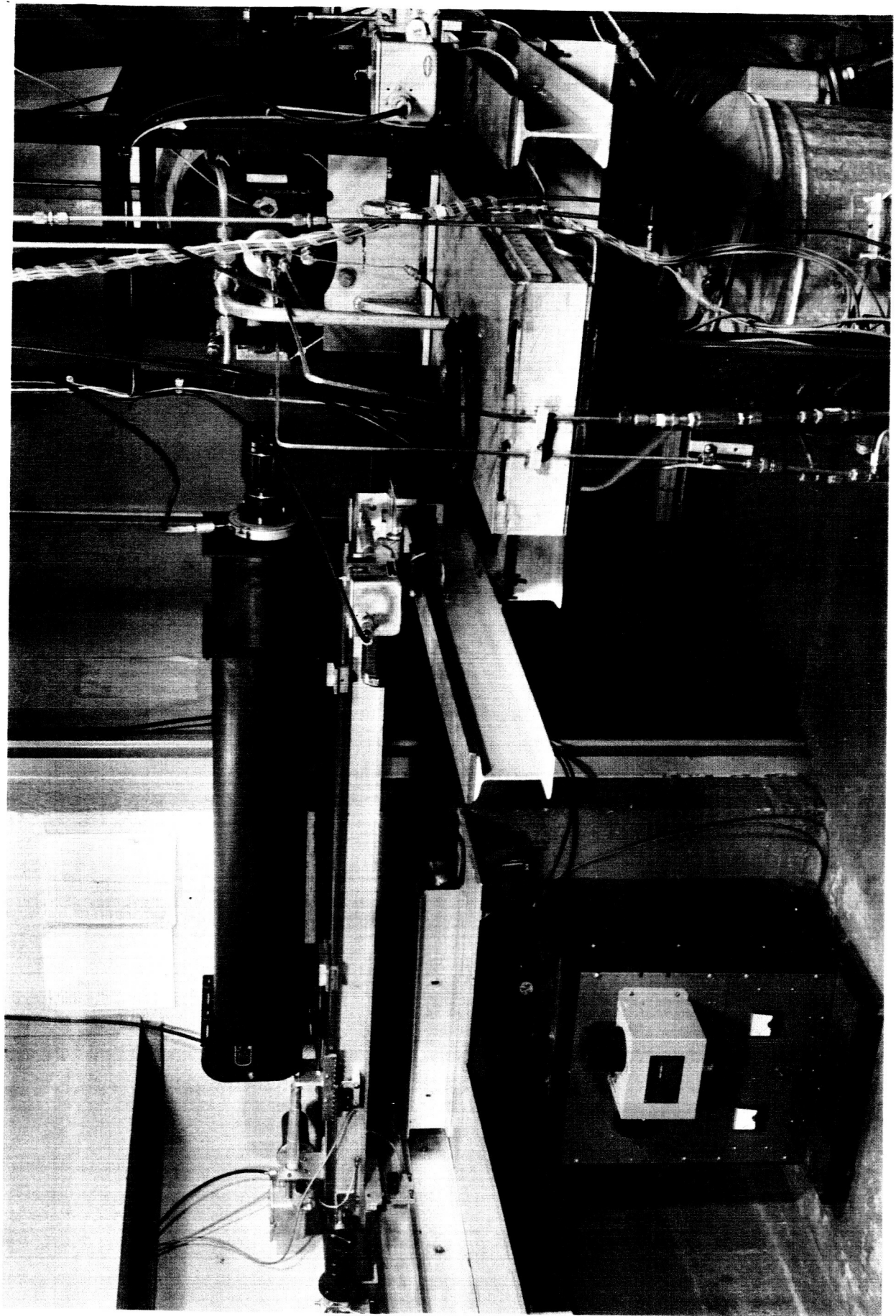
in undesirable scatter. However, this work has achieved the further development of the apparatus, a standardization of the data reduction and processing procedures and the completion of a survey of spray characteristics under various testing condition and parameters. Now that this has been achieved the work can be continued in an attempt to statistically verify these results and to obtain more qualitative information.

X. REFERENCES

- 1 Nukiyama, S. and Tanasawa, Y., "Experiments on the Atomization of Liquids in an Air Stream", Reports 1 to 6, Canada National Research Council Translations No tt-575 from Transactions of the Society of Mechanical Engineers (Japan), volumes 4, 5, 6, 1938-1940.
- 2 Crocco, L., Harrje, D. T., Sirignano, W. A., Lee, D. T., Strahle, W. C., Zinn, B. T., Mitchell, C. E., Gartner, E. M., and Gary, D. A., "Nonlinear Aspects of Combustion Instability in Liquid Propellant Rocket Motors", Princeton University Aeronautical Engineering Report 553d, June 1, 1964.
- 3 Ingebo, R. D., "Photomicrographic Tracking of Ethanol Drops in a Rocket Chamber Burning Ethanol and Liquid Oxygen", NASA D-290, June 1960.
- 4 Probert, R. P., "The Influence of Spray Particle Size and Distribution in the Combustion of Oil Droplets", Phil. Magazine, series 7, volume 37, No. 265, February 1946, pp 94-105.
- 5 Mugele, R. A., and Evans, H. G., "Droplet Size Distribution in Sprays", Industrial and Engineering Chemistry, volume 43, No. 6, June 1951, pp 1317-1324.
- 6 Hatch, T., and Choate, S. P., "Statistical Description of the Size Properties of Non-uniform Particulate Substances", Journal of the Franklin Institute, volume 207, March 1929, pp 369-387.
- 7 Foster, H. H., and Heidmann, M. F., "Spatial Characteristics of Water Sprays formed by Two Impinging Jets at Several Jet Velocities in Quiescent Air", NASA D-301, July 1960.
- 8 Mack, J. E. and Martin, M. J., "The Photographic Process", First Edition, McGraw Hill, 1939.
- 9 Bevans, R. S., "Mathematical Expressions for Drop Size Distributions in Sprays", Conference on Fuel Sprays, University of Michigan, Ann Arbor, Michigan, March 30-31, 1949.
- 10 Dobbins, R. A., "Light Scattering and Transmission Properties of Sprays", PhD Thesis, Princeton University, 1960, p 79.
- 11 Ingebo, R. D., "Drop-Size Distribution for Impinging-Jet breakup in Airstreams Simulating the Velocity Conditions in Rocket Combustors", NACA TN-4222, March 1958.
- 12 Ingebo, R. D., and Foster, H. H., "Drop-Size Distribution for Cross-current Breakup of Liquid Jets in Airstreams", NACA TN-4087, October 1957.
- 13 Heidmann, M. F., and Foster, H. H., "Effects of Impingement Angle on Drop-Size Distribution and Spray Pattern of Two Impinging Water Jets", NASA D-872, July 1961.

- 14 Reba, I., and Coleman, B., "Combustion Instability: Liquid Stream and Droplet Behavior", Aeronautical Research Laboratories, Wright-Patterson Air Force Base, WADC 59-720, September 1960.
- 15 Strahle, W. C., and Crocco, L., "Analytical Investigation of Several Mechanisms of Combustion Instability", (Bulletin of the Fifth Liquid Propulsion Symposium, November 13-15, 1963), Chemical Propulsion Information Agency.
- 16 Heidmann, M. F., Priem, R. J., and Humphrey, J. C., "A Study of Sprays Formed by Two Impinging Jets", NACA TN-3835, March 1957.

JP 21- P12-65



Resonating chamber, light receiving, and light source systems

Figure I

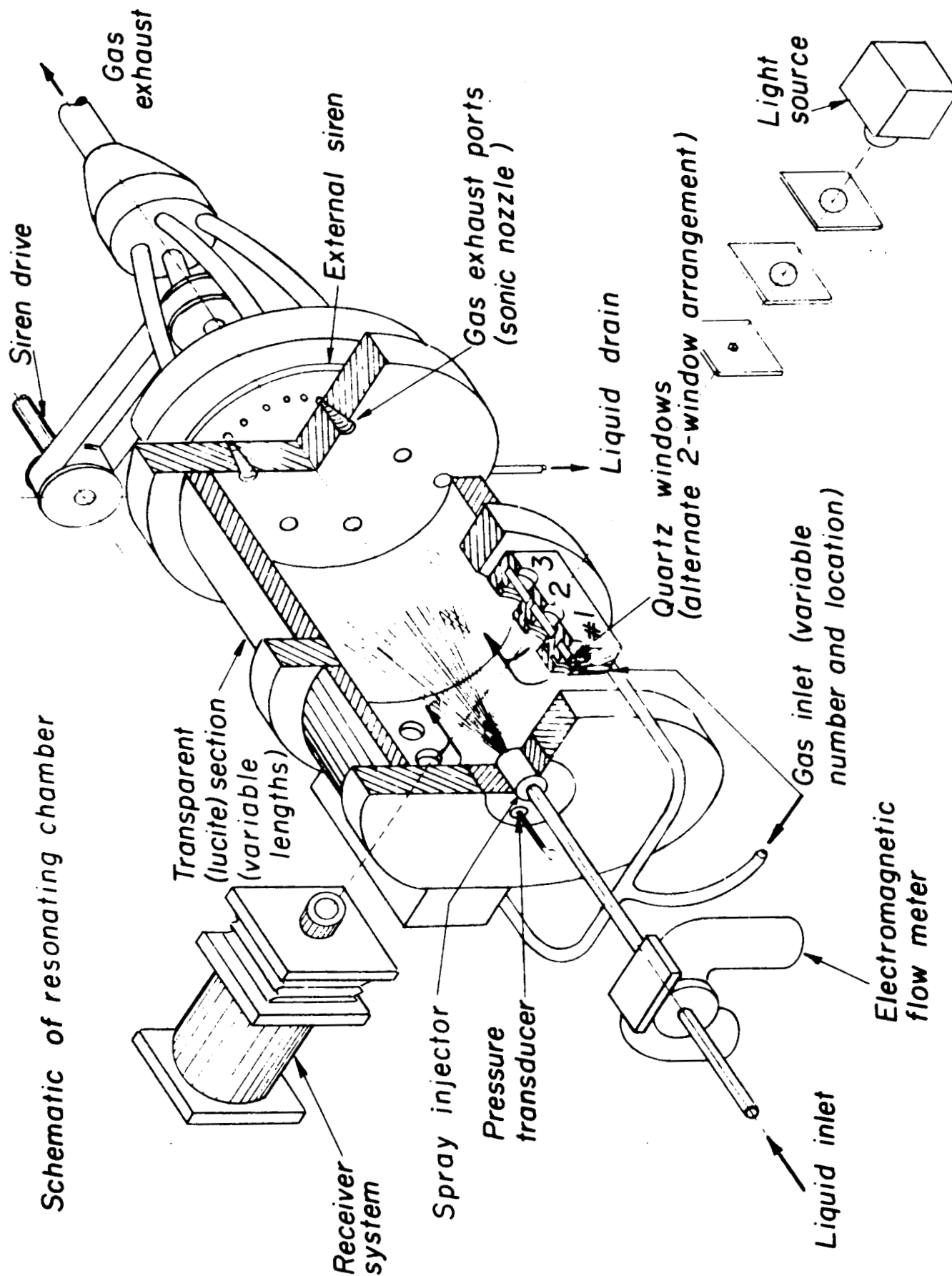
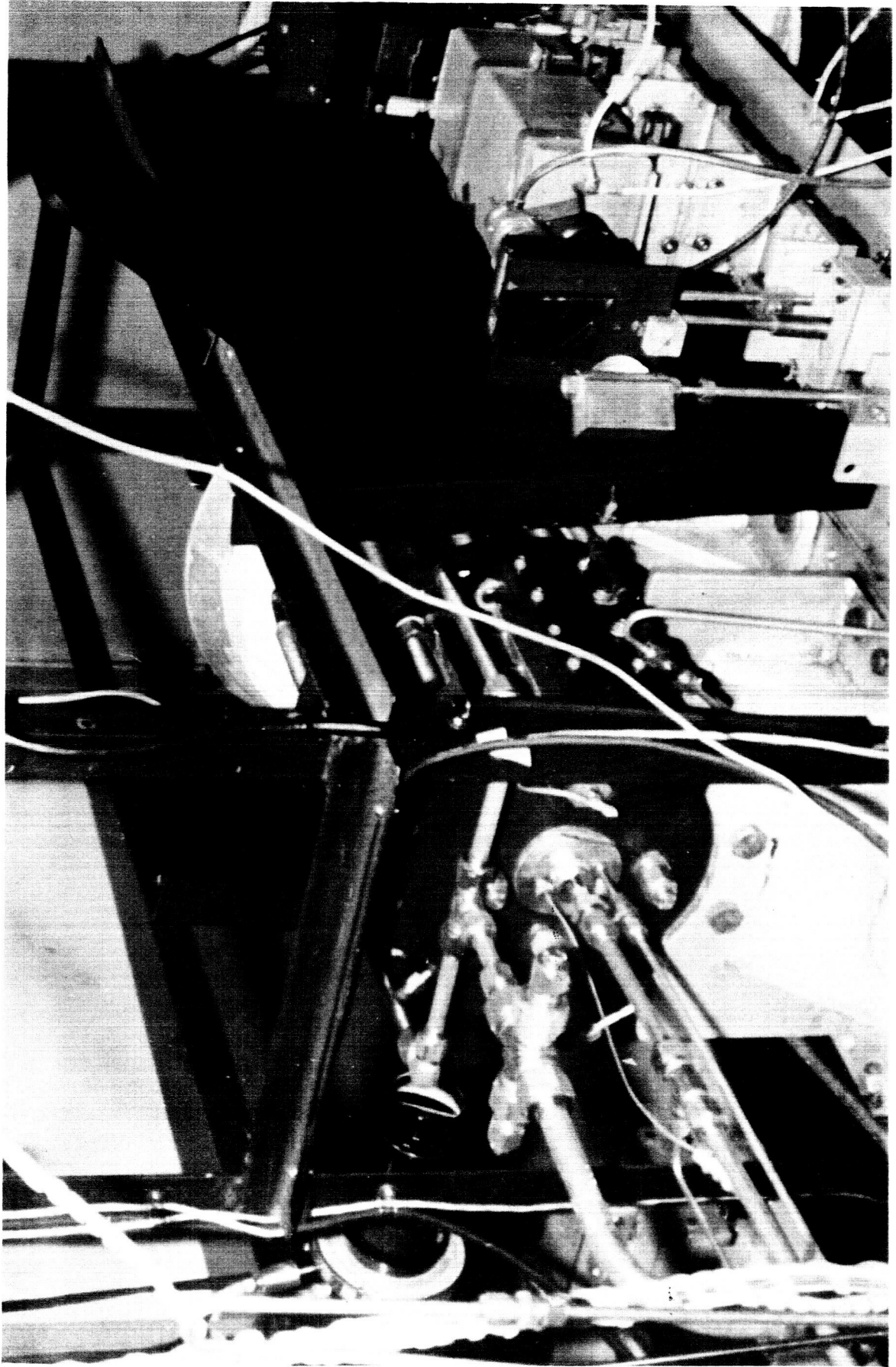


Figure 2

JP21-P26-66



Close-up of resonant chamber

Impinging jet injector element

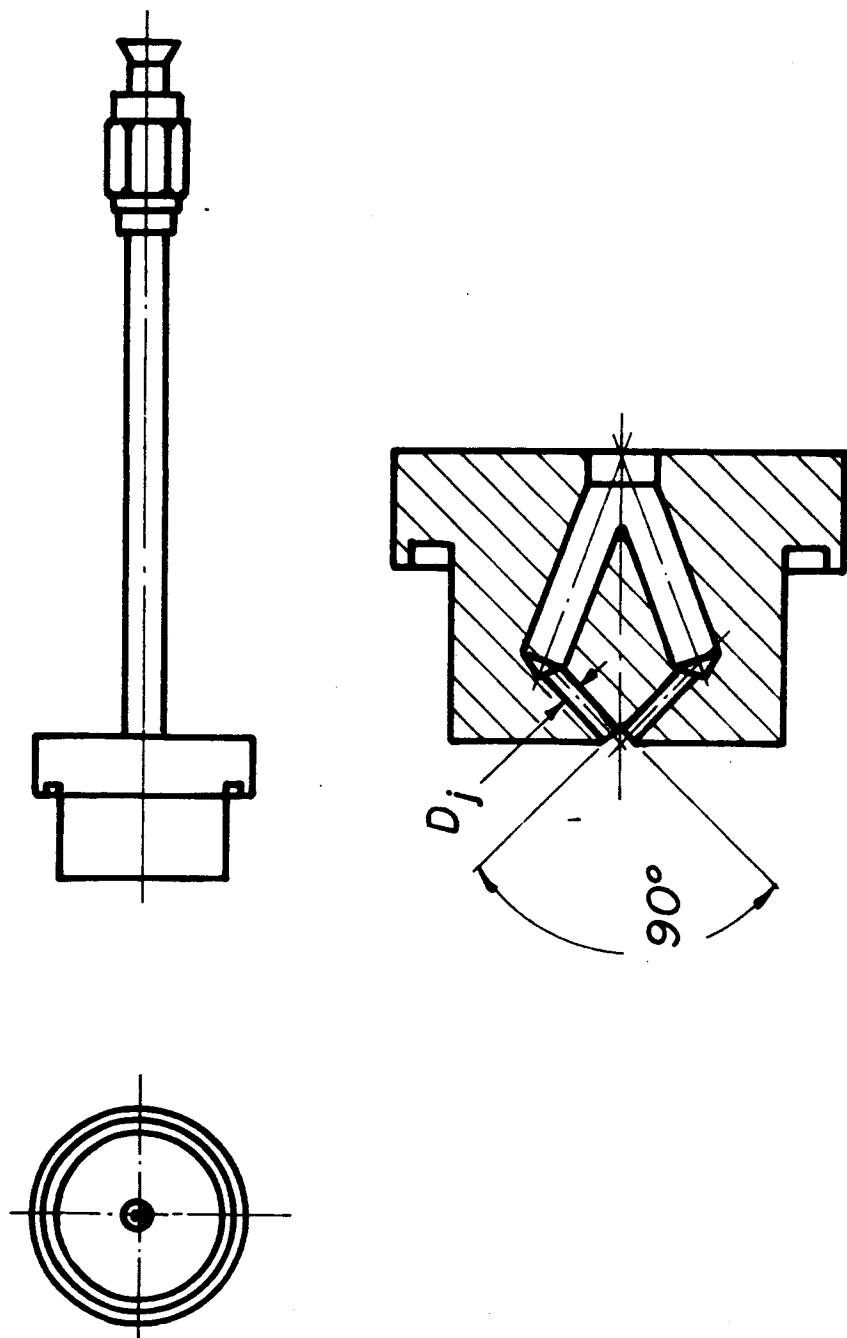


Figure 4

Comparative Fit of Three Basic Equations and D₃₀ Information

on All Distributions

Dist.	Best Curve Fits						D ₃₀ (microns)			
	Probability			Nukiyama Tanasawa			Probability Curves		Actual	*
	Upper Limit		Log							
	Error	s	Error	Error	p̄	q	Log	U.L.		
0	30	3/4	18	23	3	1	168	129	161	157
10	24	5/9	25	24	2	1	254	196	202	182
20	10	3/10	27	17	1	1	181	109	116	138
30	19	4/9	24	18	1	1	198	133	153	157
40	16	3/10	25	18	1	1	197	123	145	157
50	25	4/9	36	24	1	1½	133	110	116	138
60	28	3/10	35	22	1	½	163	107	153	182
70	27		21	22	1	½	363	301	240	560
80	19		18	19	2	½	145	59	67	560
90	18		20	17	1	1	256	184	187	214
100	10		19	17	1	1	304	198	195	214
110	17		22	19	1	1	271	212	186	214
120	33		26	27	1	½	261	77	192	214
130	28		21	18	1	½	244	108	164	182
140	9		17	15	1	½	308	202	201	284
150	8		18	16	1	½	327	214	205	214
160	19		23	21	1	½	301	204	204	284
170	46	3/4	44	42	2	½	127	92	191	560
180	38	4/9	48	44	1	1½	122	103	176	560
190	23	3/4	15	18	3	1½	258	210	229	214
200	18	5/9	18	16	2	1½	298	239	233	214
210	18	3/10	17	16	1	½	309	184	188	214
220	38	5/9	27	32	2	1	190	158	187	214
230	23	3/10	24	20	1	1	209	153	165	182
240	40	3/4	34	36	3	1	216	142	190	182
250	33		31	32	3	1	240	181	200	182
266	44		35	39	3	1½	172	141	159	147
276	51		37	40	3	1½	143	125	153	147
286	49		38	40	3	1½	195	159	170	147
290	20	5/9	14	17	3	1	284	231	233	284
306	59		46	52	3	1½	115	121	140	147
310	32	4/9	22	22	3	½	181	100	142	182
320	41	3/10	30	32	1	½	190	87	161	182
330	30	4/9	20	23	3	½	204	68	168	182
340	35		27	29	3	½	205	68	161	182

* Based on an estimated gas velocity of 5 ft/sec

FIGURE 5

Upper limit probability constants for all distribution

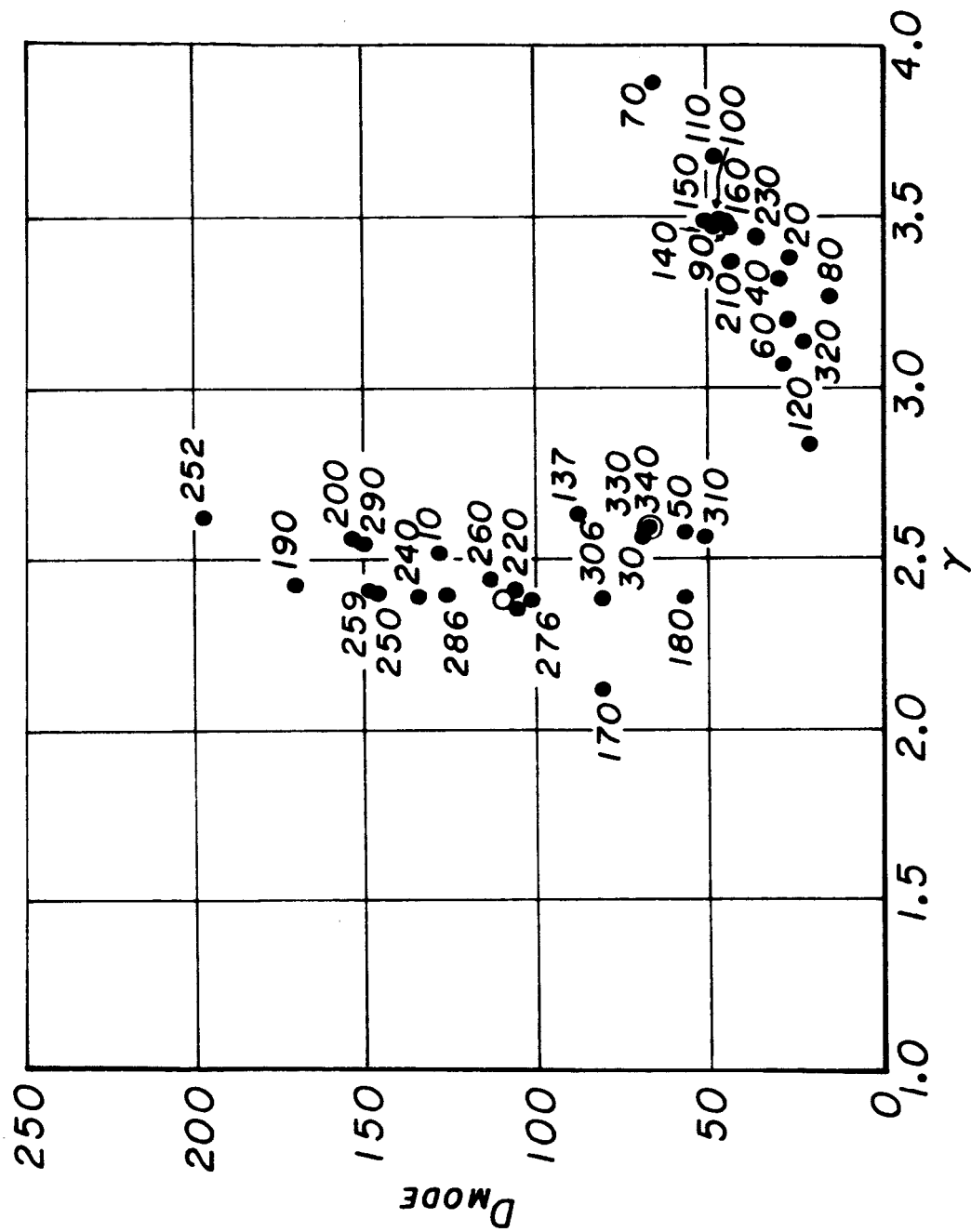


Figure 6

Summary of Test Conditions, Total Count and Values of Best Upper Limit

Probability Curve Fit for All Distributions

Dist.	D_j (In.)	x (In.)	ΔP Psi	P_c Psi	Phase ⊗ Angle	Total ‡ Count	Best Upper Limit Fit				
							c	D_{mode}	γ	D_{max}	s
0	.040	2.13	50	100	112	2039	.0071	107	2.35	269	3/4
10		3.75			151	1550	.0044	128	2.51	447	5/9
20		.50			212	1280	.0071	27	3.38	272	3/10
30		2.13			248	1493	.0057	69	2.56	332	4/9
40					—	1383	.0062	30	3.32	307	3/10
50		.50			—	1435	.0070	57	2.57	272	4/9
60		3.75			209	1135	.0088	27	3.20	277	3/10
70	.170		13		223	183	.0031	66	3.90	673	
80			11		—	595	.0126	15	3.27	151	
90	.059		50		245	1085	.0044	44	3.46	448	
100	2(.059)				144	872	.0041	47	3.48	481	
110					252	594	.0041	49	3.67	497	
120					—	438	.0077	21	2.83	221	
130	.040				—	1154	.0063	28	3.07	284	
140	.120				—	581	.0040	48	3.47	493	
150	.059				—	1235	.0038	51	3.49	515	
160	.120				160	955	.0040	49	3.47	498	
170	.170		11		—	519	.0086	81	2.12	204	3/4
180			13		194	507	.0065	57	2.38	272	4/9
190	2(.059)		50		—	1490	.0046	171	2.42	431	3/4
200					—	1290	.0057	155	2.55	541	5/9
210	.059				245	1035	.0042	44	3.37	452	3/10
220					166	2035	.0032	106	2.41	371	5/9
230	.040				173	1765	.0032	37	3.44	373	3/10
240					—	2525	.0057	135	2.39	340	3/4
250			100		—	1840	.0053	147	2.40	372	
266					151	2662	.0069	114	2.43	283	
276					194	3860	.0076	102	2.39	258	
286					194	3960	.0062	127	2.39	321	
290	.120		50		144	692	.0038	150	2.34	523	5/9
306	.040		100		—	4346	.0067	82	2.38	287	
310			50		—	1039	.0075	52	2.56	251	4/9
320					—	534	.0081	22	3.13	229	3/10
330				10	—	767	.0059	68	2.38	325	4/9
340				10	—	323	.0059	68	2.59	324	
137	Same conditions as Dist.130 & 240					1840	.0046	89	2.64	424	
252	Same conditions as Dist.250 *					1620	.0051	198	2.62	396	1
257	Same conditions as Dist.250 *					1428	.0051	150	2.40	380	3/4

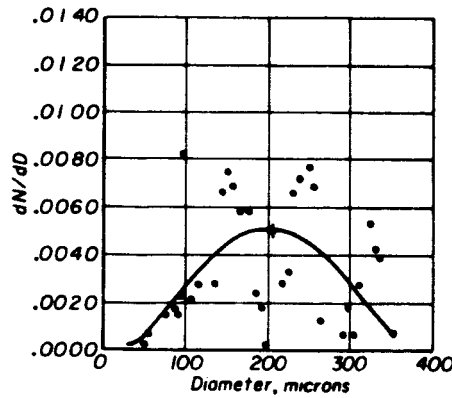
* Distributions 252 and 257 were made from the same section of a larger photograph. This section is one quarter of the complete photograph used to obtain Distribution 250.

‡ This count has been corrected for zones in the photograph where droplet images were obscured. It is a count per complete photograph.

⊗ Phase angle of chamber pressure oscillation as monitored at the injector end of the chamber. Steady-state runs are marked with —.

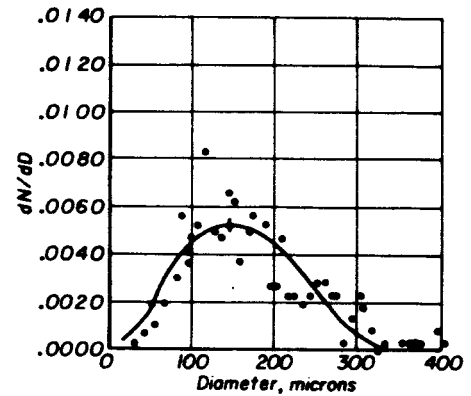
FIGURE 7

Droplet number - size distributions for various testing conditions



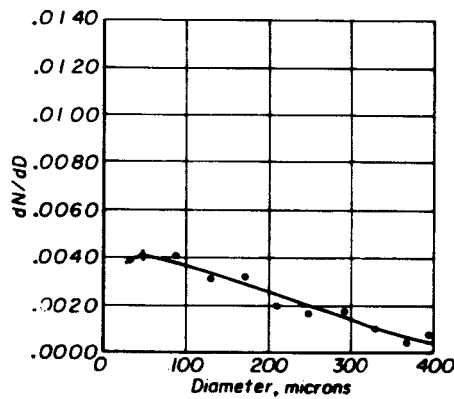
Upper-limit probability distribution
252

Original count



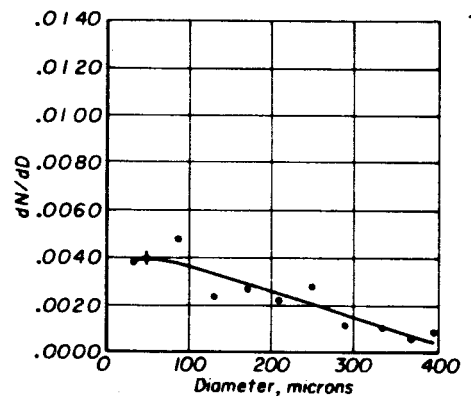
Upper-limit probability distribution
257

Recount



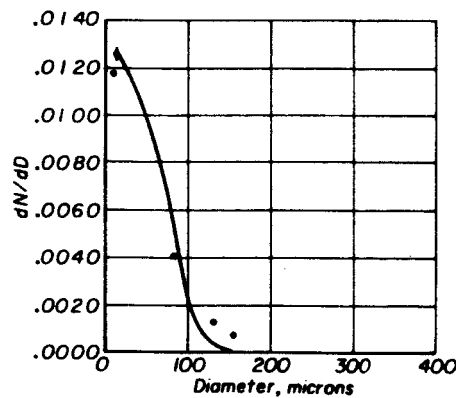
Upper-limit probability distribution
140

Steady-state, .120"



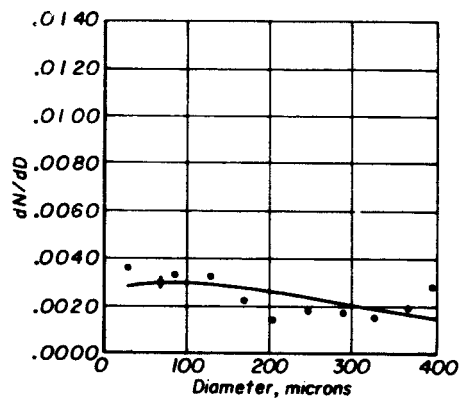
Upper-limit probability distribution
160

Oscillating pressure, .120"



Upper-limit probability distribution
80

High count, .170"

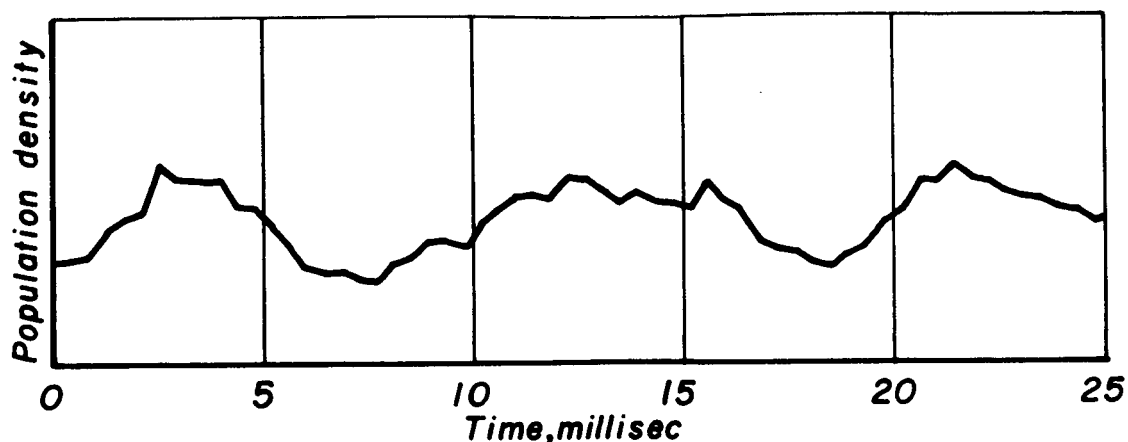


Upper-limit probability distribution
70

Low count, .170"

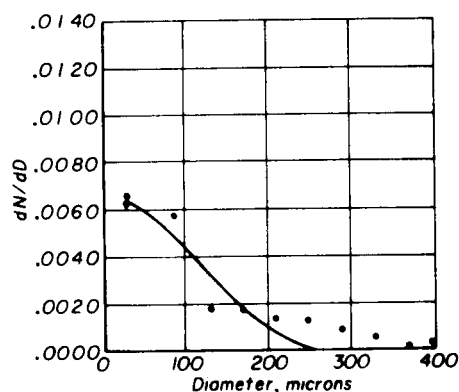
JP21-R4035-LS

Figure 8

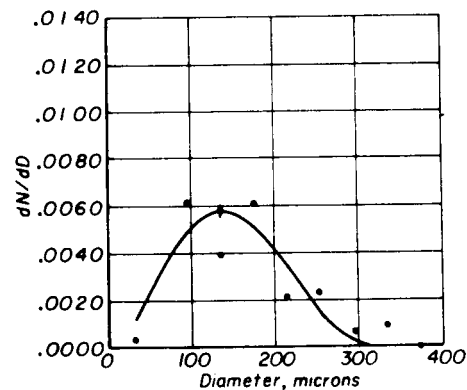


Relative density of droplet waves under standard test condition

Droplet number - size distributions for various testing conditions



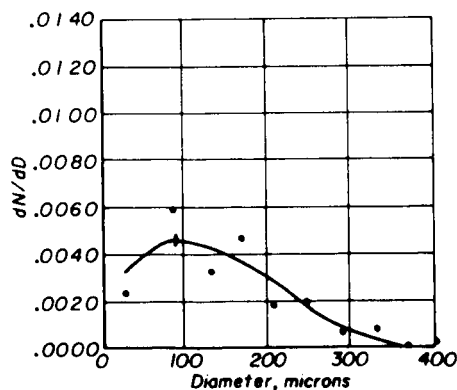
Upper-limit probability distribution
130



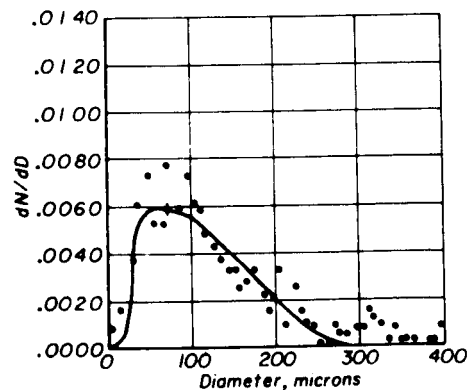
Upper-limit probability distribution
240

Low count, .040" inj., $P_c = 100$ psig

High count, .040" inj., $P_c = 100$ psig



Upper-limit probability distribution
137



Upper-limit probability distribution
330

Sum of distributions 130 + 240

.040" inj., $P_c = 10$ psig

Figure 9

DISTRIBUTION FOR THIS REPORT

NASA

NASA Headquarters
Washington, D.C. 20546
Attn: Alfred Gessow
J. Suddreth (3)
A.O. Tischler RP

NASA
Universal North Building
Connecticut & Florida Avenues
Washington, D.C.
Attn: T.L. Smull, Director
Grants & Space Contracts (10)

NASA Scientific & Technical
Information Facility
P.O. Box 33
College Park, Maryland 20740 (15)

NASA Headquarters
Washington, D.C. 20546
Attn: E.L. Gray, Director
Advanced Manned Missions, MT
Office of Manned Space Flight

Attn: V.L. Johnson, Director
Launch Vehicles & Propulsion, SV
Office of Space Science

Ames Research Center
Moffett Field
California 94035
Attn: Technical Librarian
Designee: Harold Hornby
Mission Analysis Division

Goddard Space Flight Center
Greenbelt, Maryland 20771
Attn: Technical Librarian
Designee: Merland L. Moseson
Code 620

Jet Propulsion Laboratory
California Institute of Technology
4800 Oak Grove Drive
Pasadena, California 91103
Attn: J.H. Rupe
Attn: Technical Librarian
Designee: Henry Burlage, Jr.
Propulsion Div., 38

Langley Research Center
Langley Station
Hampton, Virginia 23365
Attn: Technical Librarian
Designee: Floyd L. Thompson, Director

NASA
Lewis Research Center
21000 Brookpark Road
Cleveland, Ohio 44135
Attn: M.F. Heidmann (Technical Monitor)
R.J. Priem
E. Conrad

Attn: Technical Librarian
Designee: A. Silverstein, Director

Manned Spacecraft Center
Houston, Texas 77001
Attn: G. Spencer

Attn: Technical Librarian
Designee: Robert R. Gilruth, Director

Marshall Space Flight Center
R-P&VED
Huntsville, Alabama 35812
Attn: Jerry Thomson
R.J. Richmond

Attn: Technical Librarian
Designee: Hans G. Paul

GOVERNMENT INSTALLATIONS

Headquarters, U.S. Air Force
Washington 25, D.C.
Attn: Technical Librarian
Designee: Col. C.K. Stambaugh
AFRST

Aeronautical Systems Division
Air Force Systems Command
Wright-Patterson Air Force Base
Dayton, Ohio 45433
Attn: Technical Librarian
Designee: D.L. Schmidt
Code ASRCNC-2

Air Force Missile Test Center
Patrick Air Force Base
Florida
Attn: Technical Librarian
Designee: L.J. Ullian

Air Force Office of Scientific Research
Propulsion Division
Washington, D.C.
Attn: B.T. Wolfson

Air Force Rocket Propulsion Laboratory
Research & Technology Division
Air Force Systems Command
Edwards, California 93523
Attn: R.R. Weiss, RPRR

Attn: Technical Librarian
Designee: H. Main

Air Force Systems Division
Air Force Unit Post Office
Los Angeles 45, California
Attn: Technical Librarian
Designee: Col. Clark
Technical Data Center

ARL (ARC)
Building 450
Wright-Patterson Air Force Base
Dayton, Ohio
Attn: K. Scheller

Arnold Engineering Development Center
Arnold Air Force Station
Tullahoma, Tennessee
Attn: Technical Librarian
Designee: H.K. Doetsch

Department of the Navy
Bureau of Naval Weapons
Washington, D.C.
Attn: Technical Librarian
Designee: J. Kay
RTMS-41

Department of the Navy
Office of Naval Research
Washington, D.C. 20360
Attn: R.O. Jackel

Defense Documentation Center Headquarters
Cameron Station, Building 5
5010 Duke Street
Alexandria, Virginia 22314
Attn: TISIA

Picatinny Arsenal
Dover, New Jersey 07801
Attn: E. Jenkins

Attn: Technical Librarian
Designee: I. Forsten, Chief
Liquid Propulsion Laboratory
SMUPA-DL

Redstone Scientific Information
Building 4484
Redstone Arsenal
Huntsville, Alabama
Attn: Technical Library

RTNT
Bolling Field
Washington, D.C. 20332
Attn: L. Green, Jr.

U.S. Army Missile Command
Redstone Arsenal
Alabama 35809
Attn: J. Connaughton

Attn: Technical Librarian
Designee: Walter Wharton

U.S. Atomic Energy Commission
Technical Information Services
Box 62
Oak Ridge, Tennessee
Attn: Technical Librarian
Designee: A.P. Huber
Gaseous Diffusion Plant
(ORGDP) P.O. Box P

U.S. Naval Ordnance Test Station
China Lake
California 93557
Attn: E.W. Price

Attn: Technical Librarian
Designee: Code 4562
Chief, Missile Propulsion Div.

CPIA

Chemical Propulsion Information Agency
Applied Physics Laboratory
The John Hopkins University
8621 Georgia Avenue
Silver Spring, Maryland 20910
Attn: T.W. Christian

Attn: Technical Librarian
Designee: Neil Safeer

INDUSTRY CONTRACTORS

Aerojet-General Corporation
P.O. Box 296
Azusa, California 91703
Attn: Technical Librarian
Designee: L.F. Kohrs

Aerojet-General Corporation
P.O. Box 1947
Sacramento, California 95809
Attn: R.J. Hefner
F.H. Reardon
Attn: Technical Librarian
Bldg. 2015, Dept. 2410
Designee: R. Stiff

Aeronutronic
Philco Corporation
Ford Road
Newport Beach, California 92663
Attn: Technical Librarian
Designee: D.A. Carrison

Aerospace Corporation
P.O. Box 95085
Los Angeles, California 90045
Attn: O.W. Dykema
W.C. Strahle

Attn: Technical Librarian
Designee: John G. Wilder
MS-2293
Propulsion Dept.

Astrosystems International, Inc.
1275 Bloomfield Avenue
Fairfield, New Jersey 07007
Attn: Technical Librarian
Designee: A. Mendenhall

Atlantic Research Corporation
Edsall Road and Shirley Highway
Alexandria, Virginia 22314
Attn: Technical Librarian
Designee: A. Scurlock

Battelle Memorial Institute
505 King Avenue
Columbus 1, Ohio
Attn: Charles E. Day,
Classified Rept. Librarian

Bell Aerosystems Company
P.O. Box 1
Buffalo 5, New York 14240
Attn: T. Rossman
J. Senneff

Attn: Technical Librarian
Designee: W.M. Smith

Boeing Company
P.O. Box 3707
Seattle, Washington 98124
Attn: Technical Librarian
Designee: J.D. Alexander

Chrysler Corporation
Missile Division
P.O. Box 2628
Detroit, Michigan 48231
Attn: Technical Librarian
Designee: John Gates

Curtiss-Wright Corporation
Wright Aeronautical Division
Wood-Ridge, New Jersey 07075
Attn: Technical Librarian
Designee: G. Kelley

Defense Research Corporation
6300 Hollister Avenue
P.O. Box 3587
Santa Barbara, California 93105
Attn: B. Gray
C.H. Yang

Douglas Aircraft Company
Missile & Space Systems Division
3000 Ocean Park Boulevard
Santa Monica, California 90406
Attn: Technical Librarian

Designee: R.W. Hallet
Advanced Space Tech.

Douglas Aircraft Company
Astropower Laboratory
2121 Paularino
Newport Beach, California 92663
Attn: Technical Librarian
Designee: George Moc
Director, Research

Dynamic Science Corporation
1445 Huntington Drive
South Pasadena, California
Attn: M. Gerstein

General Dynamics/Astronautics
Library & Information Services (128-00)
P.O. Box 1128
San Diego, California 92112
Attn: Technical Librarian
Designee: Frank Dore

General Electric Company
Advanced Engine & Technology Dept.
Cincinnati, Ohio 45215
Attn: Technical Librarian
Designee: D. Suichu

General Electric Company
Malta Test Station
Ballston Spa, New York
Attn: Alfred Graham, Manager
Rocket Engines

General Electric Company
Re-Entry Systems Department
3198 Chestnut Street
Philadelphia, Pennsylvania 19101
Attn: Technical Librarian
Designee: F.E. Schultz

Geophysics Corporation of America
Technical Division
Bedford, Massachusetts
Attn: A.C. Toby

Grumman Aircraft Engineering Corp.
Bethpage
Long Island, New York
Attn: Technical Librarian
Designee: Joseph Gavin

Ling-Temco-Vought Corporation
Astronautics
P.O. Box 5907
Dallas, Texas 75222
Att: Technical Librarian
Designee: Warren C. Trent

Arthur D. Little, Inc.
20 Acorn Park
Cambridge, Massachusetts 02140
Attn: E. Karl Bastress
Attn: Technical Librarian

Lockheed Missiles & Space Co.
P.O. Box 504
Sunnyvale, California 94088
Attn: Technical Information Center
Designee: Y.C. Lee

Lockheed Propulsion Company
P.O. Box 111
Redlands, California 91409
Attn: Technical Librarian
Designee: H.L. Thackwell

McDonnell Aircraft Corporation
P.O. Box 516
Municipal Airport
St. Louis, Missouri 63166
Attn: Technical Librarian
Designee: R.A. Herzmark

The Marquardt Corporation
16555 Saticoy Street
Van Nuys, California 91409
Attn: Technical Librarian
Designee: Warren P. Boardman, Jr.

Martin Marietta Corporation
Denver Division
P.O. Box 179
Denver, Colorado 80201
Attn: Technical Librarian
Designee: J.D. Goodlette (A-241)

Multi-Tech. Inc.
Box 4186 No. Annex
San Fernando, California
Attn: F.B. Cramer

Northrup Space Laboratories
3401 West Broadway
Hawthorne, California
Attn: Technical Librarian
Designee: William Howard

Rocket Research Corporation
520 South Portland Street
Seattle, Washington 98108
Attn: Technical Librarian
Designee: Foy McCullough, Jr.

Rocketdyne
Division of North American Aviation
6633 Canoga Avenue
Canoga Park, California 91304
Attn: R. Fontaine
R.B. Lawhead
R.S. Levine

Attn: Technical Librarian
(Library 586-306)
Designee: E.B. Monteath

Space & Information Systems Division
North American Aviation, Inc.
12214 Lakewood Boulevard
Downey, California 90241
Attn: Technical Librarian
Designee: H. Storms

Rohm & Haas Company
Redstone Arsenal
Huntsville, Alabama
Attn: Librarian

Stanford Research Institute
333 Ravenswood Avenue
Menlo Park, California 94025
Attn: Technical Librarian
Designee: Lionel Dickinson

Thiokol Chemical Corporation
Huntsville Division
Huntsville, Alabama
Attn: Technical Librarian
Designee: John Goodloe

Thiokol Chemical Corporation
Reaction Motors Division
Denville, New Jersey 07832
Attn: D. Mann

Attn: Technical Librarian
Designee: Arthur Sherman

TRW Systems
One Space Park
Redondo Beach, California 90278
Attn: G.W. Elverum
Attn: Donald H. Lee
Attn: Technical Librarian

United Technology System
Division of United Aircraft Corporation
P.O. Box 358
Sunnyvale, California 94088
Attn: R.H. Osborn
Attn: Technical Librarian

Pratt & Whitney Aircraft Company
Division of United Aircraft Corp.
West Palm Beach
Florida
Attn: G. Lewis

Pratt & Whitney Aircraft Company
Division of United Aircraft Corp.
Engineering, Building 1-F
East Hartford, Connecticut
Attn: D.H. Utvik

Research Laboratories
Division of United Aircraft Corp.
400 Main Street
East Hartford, Connecticut 06108
Attn: Technical Librarian
Designee: Erle Martin

Walter Kidde and Company
Aerospace Operations
567 Main Street
Belleville, New Jersey 07109
Attn: Technical Librarian
Designee: R.J. Hanville
Director of Research Eng.

Warner-Swasey Company
Control Instrument Division
32-16 Downing Street
Flushing, New York 11354
Attn: R.H. Tourin

UNIVERSITIES

California Institute of Technology
204 Karman Laboratory
Pasadena, California 91109
Attn: Fred E. Culick

Dartmouth University
Hanover
New Hampshire
Attn: P.D. McCormack

Georgia Institute of Technology
Aerospace School
Atlanta 13
Georgia
Attn: Ben T. Zinn

Illinois Institute of Technology
10 W. 35th Street
Chicago, Illinois
Attn: P.T. Torda

The John Hopkins University
Applied Physics Laboratory
8621 Georgia Avenue
Silver Spring, Maryland
Attn: W.G. Berl

Massachusetts Institute of Technology
Cambridge 39
Massachusetts
Attn: T.Y. Toong
Dept. of Mechanical Engineering
Attn: Gail E. Partridge, Librarian
Engineering Projects Laboratory

New York University
Dept. of Chemical Engineering
New York 53, New York
Attn: P.F. Winternitz

Ohio State University
Rocket Research Laboratory
Dept. of Aeronautical & Astronautical Eng.
Columbus 10, Ohio
Attn: Technical Librarian

Polytechnic Institute of Brooklyn
Graduate Center
Route 110
Farmingdale, New York
Attn: V.D. Agosta

Purdue University
School of Mechanical Engineering
Lafayette, Indiana
Attn: J.R. Osborn

University of California
Institute of Engineering Research
Berkeley, California
Attn: A.K. Oppenheim

University of Michigan
Aeronautical & Astronautical Eng. Labs.
Aircraft Propulsion Lab.
North Campus
Ann Arbor, Michigan
Attn: J.A. Nicholls

University of Wisconsin
Dept. of Mechanical Engineering
1513 University Avenue
Madison, Wisconsin
Attn: P.S. Myers

Yale University
Dept. of Engineering & Applied Science
Mason Laboratory
400 Temple Street
New Haven, Connecticut
Attn: B.T. Chu